DISSERTATION

FDOA-BASED PASSIVE SOURCE LOCALIZATION: A GEOMETRIC PERSPECTIVE

Submitted by

Karleigh J. Cameron

Department of Mathematics

In partial fulfillment of the requirements

For the Degree of Doctor of Philosophy

Colorado State University

Fort Collins, Colorado

Fall 2018

Doctoral Committee:

Advisor: Dan Bates

Margaret Cheney
Chris Peterson
Bailey Fosdick

ABSTRACT

FDOA-BASED PASSIVE SOURCE LOCALIZATION: A GEOMETRIC PERSPECTIVE

We consider the problem of passively locating the source of a radio-frequency signal using observations by several sensors. Received signals can be compared to obtain time difference of arrival (TDOA) and frequency difference of arrival (FDOA) measurements. The geometric relationship satisfied by these measurements allow us to make inferences about the emitter's location. In this research, we choose to focus on the FDOA-based source localization problem. This problem has been less widely studied and is more difficult than solving for an emitter's location using TDOA measurements. When the FDOA-based source localization problem is formulated as a system of polynomials, the source's position is contained in the corresponding algebraic variety. This provides motivation for the use of methods from algebraic geometry, specifically numerical algebraic geometry (NAG), to solve for the emitter's location and gain insight into this system's interesting structure.

ACKNOWLEDGEMENTS

I have the deepest gratitude for all those who have encouraged me and supported me throughout this journey.

Thank you to my advisor, Dan, for seeing my potential and for being such a calm and patient mentor through hours of meetings and editing. Working with you has made my time at CSU great. You are a role model for many and it is a privilege to be your student.

Thank you to Margaret Cheney for introducing me to the interesting area of source localization and signal processing. Your passion for connecting the engineering and mathematics communities and solving interesting real-world problems is infectious.

I was fortunate to participate in several summer research programs and so I thank my mentors, Manjula Ambur, Jeremy Yagle, Ben Robinson, and Dan Janning. The things you all taught me made me a more well-rounded researcher and motivated me to pursue a career in industry.

Thank you to my parents for being my biggest cheerleaders and keeping me sane through countless stressed-out phone calls and "career crises". Your unwavering belief in me from the beginning and encouragement to pursue whatever goals I set my mind to has made a bigger impact than you know.

To Sam, thank you for being my partner in everything. My life is forever better because we both chose to move to Colorado. It is a privilege to be completing this journey with you.

I will always look upon my time at CSU as some of the best years of my life, largely due to the life-long friends I have made here. To all of you, thanks for making Fort Collins home to me. Grad school can be stressful, but the friendship and camaraderie that comes out of it is incredibly special. I will cherish every memory of wine and cheese nights, Mugs runs, inner-tube water polo games (go Sitting Ducks!), spring breaks in Utah, office shenanigans, and countless others. I will miss you all and consider myself fortunate to have built relationships that make parting ways so difficult.

Funding acknowledgements: This research was supported by NSF grant DMS-1719658 and AFOSR grant FA9550-14-1-0185.

TABLE OF CONTENTS

LIST OF TABLES

LIST OF FIGURES

Chapter 1

Introduction

In the fields of radar, sonar, and acoustics it is often necessary to find the source of a signal using *passive source localization* techniques. For instance, ships in distress use a radio-frequency signal-emitting beacon to alert land-based authorities. For effective search and rescue, the location of this beacon (and thus, the ship) must be estimated [1]. In acoustics, many speech and voice recognition algorithms require knowledge of sound source position [2]. Thus, source localization techniques are required to precisely estimate the speaker's position.

A particularly widespread use for passive source localization techniques is in the area of passive radar. Traditional (active) radar detection and imaging involves a signal sent by the user being reflected off of objects in its range. Conversely, *passive* radar utilizes signals already being transmitted to make observations. This distinction is shown in Figure 1.1. In passive radar, the sources of the observed signals are often unknown and can include communication towers, Wi-Fi routers, and space-based Global Positioning Systems, among many other radio-frequency emitters [3]. To effectively utilize a signal for radar applications, it is often necessary to determine the origin of the signal being used, thus requiring source localization techniques.

Passive techniques are becoming more important as technology is increasingly prevalent. It is said that the electromagnetic spectrum is becoming 'crowded' with radiation emitted at various frequencies. This causes an increase in noise from interfering signals and limits waveform options for signal transmission. Since passive radar does not require emission of a signal by the observer, it is a promising alternative to traditional active radar techniques.

Passive source localization involves measuring an observed signal with several nearby receivers. The received signals can then be compared to obtain time difference of arrival (TDOA) and frequency difference of arrival (FDOA) quantities. TDOA measurements describe the time delays caused by separation between the receivers and the emitter. The re-

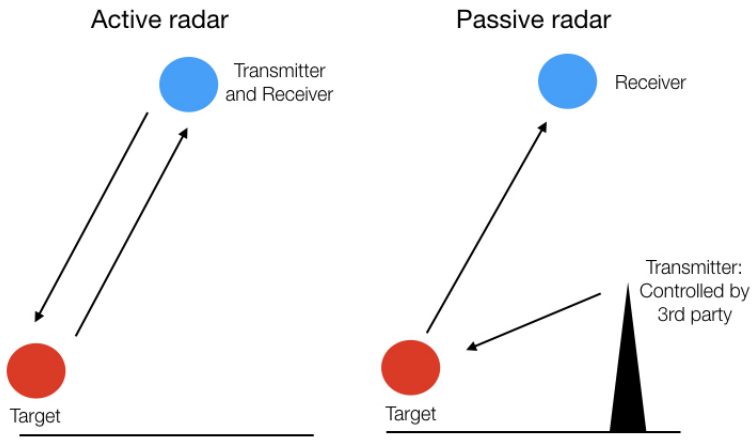

Figure 1.1: Active radar involves the sending of a signal, then receiving the waves after reflection off of a scene or target. Knowledge about the sent wave can be used to determine the location of the target or to distinguish objects in a scene. In passive radar, the user does not have knowledge about the sent signal's frequency or origin. One way to make the information usable is to determine the origin of the signal using passive source localization.

ceived signals also experience a frequency shift caused by a difference in velocity between the emitter and the receiver. This is due to the Doppler effect [4]. FDOA measurements quantify this disparity in observed signal frequency. Using these relationships, TDOA/FDOA measurements, along with receiver locations and velocities, can be used to back-out the source location.

The problem of locating an emitter using TDOA or FDOA is highly algebraic and geometric in nature. In fact, the problem can be described by a set of polynomial equations whose solution corresponds to the location of the transmitter. This suggests the use of methods from computational algebraic geometry. The FDOA-based problem in particular is highly nonlinear, which makes its solution ill-conditioned and sensitive to noise. Approaching the problem from an algebro-geometric perspective provides tools for understanding the intricate relationship between emitter location and velocity, receiver geometry and velocities, and the resulting frequency shift.

This dissertation develops methods for passive source localization using FDOA measurements, since the TDOA case has been comprehensively studied in [2, 5–14], among others. Additionally, geolocation of a source using only FDOA measurements is valuable since many

signals possess fine Doppler resolution and coarse range (TDOA) resolution. In fact, the radar ambiguity function ensures an inverse relationship between range and Doppler resolution[1] [4]. With traditional radar applications the user has control over the type of signal being transmitted, but this is not true for the passive setting. Thus, it is beneficial to possess capabilities for processing a diverse set of waveforms.

This thesis is organized as follows. A technical summary of the TDOA and FDOA-based source localization problem, along with an overview of relevant work in the area, is presented in Chapter 2. The closing paragraph outlines the objectives of this dissertation. Chapter 3 shows how the problem can be formulated as systems of polynomials, which provides natural bounds for the number of receivers necessary to obtain a zero-dimensional solution set. Framing the source-localization problem in this way also allows for the use of techniques from computational algebraic geometry, specifically utilizing numerical algebraic geometry (NAG) and elimination theory. An overview of some of these methods is provided in Chapter 4. This concludes the preliminary section.

Chapters 5, 6, and 7 detail three separate projects related to FDOA-based passive source localization. Chapter 5 presents a novel geolocation algorithm utilizing the NAG techniques presented in Section 4.1 in conjunction with the RANdom SAmpling Consensus (RANSAC) method. This algorithm combines the polynomial system solving power of the NAG software Bertini [15] with the robustness to noise of RANSAC. It is also one of only a handful of algorithms that allow for a solution to be found using only FDOA measurements.

In addition to TDOA and FDOA measurements, the direction of arrival (DOA) of a signal is a useful quantity for locating a source. In Chapter 6 the relationship between TDOA, FDOA, and direction of arrival is explored. This relationship leads to a novel technique for estimating direction of arrival from TDOA or FDOA measurements. This method utilizes a simplification arising from the far-field assumption.

[1]This is discussed further in Appendix A.

For a fixed set of system parameters, we construct a map between the location of a source and the corresponding set of FDOA measurements. A natural question to ask is: what is the *image* of this map? This corresponds to the set of all feasible FDOA measurements. Chapter 7 provides an analysis of the surface of feasible FDOA measurements and assesses its use for de-noising data. The work in this chapter employs elimination theory (specifically, the Dixon resultant) and numerical algebraic geometry.

The final chapter (Chapter 8) contains concluding remarks and a discussion of a few related projects that may be pursued in the future.

Chapter 2

Background

As was discussed in the previous chapter, this work features several approaches to understanding and exploiting the algebra and geometry of FDOA-based source localization. This chapter provides an introduction to the geolocation problem (Section 2.1) along with an overview of current work in the area.

2.1 Geolocation with TDOA and FDOA

Source localization is often performed using measurements of a signal obtained by several nearby receivers. In this thesis we do not focus on the signal processing techniques used to extract the relevant quantities from a signal, although a summary is included in Appendix A. Instead, the focus of this work is on the geolocation of a source once measurements are obtained.

In passive source localization, observers do not have information about the signal that was sent, such as its frequency or the time of transmission, but can compare the received signals to find discrepancies in frequency or time delay. This information can be used to solve for the signal's origin, using the geometric relationship between the receivers and the location of the source. Specific measurements gathered are the time difference of arrival (TDOA) and frequency difference of arrival (FDOA). Additionally, the geolocation problem can be simplified if information about the transmitter is known *a priori*, such as altitude (ALT).

This section outlines the mathematical and physical framework for geolocation using TDOA and FDOA and summarizes other relevant work in the field. The problem is formulated in three dimensions with an earth-centered, earth-fixed coordinate system (ECEF). Later in this thesis, the two-dimensional system will also be considered as a simpler case. Al-

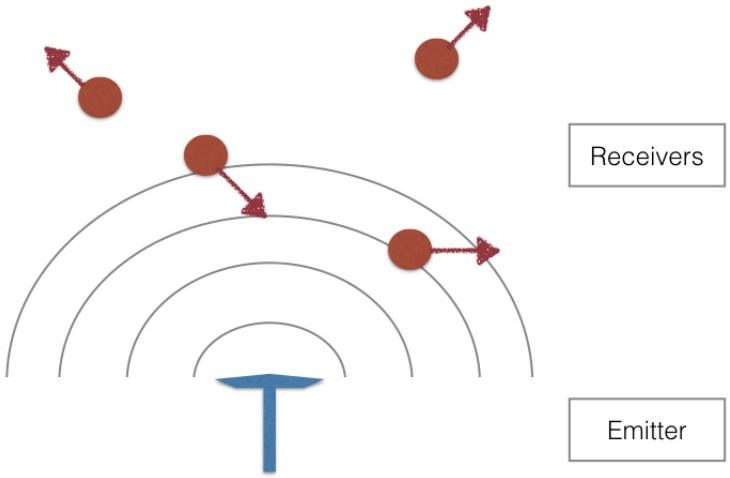

Figure 2.1: Passive source localization seeks to find the position of the emitter (blue tower), given measurements of the signal by several receivers (red circles). For FDOA-based source localization, the relative velocity between emitter and receivers must be nonzero.

though the methods developed here are relevant to a variety of scenarios, we usually assume a radio-frequency signal for consistency.

2.1.1 Time Difference of Arrival (TDOA)

Consider a transmitter at location $\mathbf{x} = (x, y, z)^T$, emitting a signal with speed of propagation c. For a radio-frequency signal in free space, c is the speed of light. There are n sensors observing the signal at locations $\mathbf{x}_1 = (x_1, y_1, z_1)^T, \ldots, \mathbf{x}_n = (x_n, y_n, z_n)^T$. The amount of time it takes the signal to travel to the i^{th} receiver is

$$\tau_i = \frac{1}{c}\|\mathbf{x}_i - \mathbf{x}\| = \frac{1}{c}\sqrt{(x_i - x)^2 + (y_i - y)^2 + (z_i - z)^2}.$$

This gives rise to the first definition.

Definition 1. *The **time difference of arrival (TDOA)**, between the first receiver and the i^{th} receiver is equivalent to*

$$\begin{aligned} c \cdot \tau_{1,i} &= \|\mathbf{x}_i - \mathbf{x}\| - \|\mathbf{x}_1 - \mathbf{x}\| \\ &= \sqrt{(x_i - x)^2 + (y_i - y)^2 + (z_i - z)^2} - \sqrt{(x_1 - x)^2 + (y_1 - y)^2 + (z_1 - z)^2}. \end{aligned} \tag{2.1}$$

This is essentially the signal lag time between receivers. The above equation can be written for all pairs of receivers, although only $n-1$ pairs will be linearly independent. This is due to the fact that the measurements should satisfy the relation:

$$\tau_{i,j} + \tau_{j,k} - \tau_{i,k} = 0.$$

Thus, without loss of generality, one can simply consider the TDOA measurements between receivers $2, ..., n$ and receiver 1. We refer to receiver 1 as the *reference receiver*.

The receiver positions $\mathbf{x}_1, \ldots, \mathbf{x}_n$ are known parameters. Thus, we frame the relation above (2.1) as the map:

$$\begin{aligned} T_3 : \ \mathbb{R}^3 &\longrightarrow \mathbb{R}^{n-1} \\ \mathbf{x} &\longrightarrow (\tau_{2,1}, \ldots, \tau_{n,1}), \end{aligned} \tag{2.2}$$

with $\tau_{i,j}$ defined as in (2.1). When provided with TDOA measurements $(\tau^*_{2,1}, \ldots, \tau^*_{n,1})$, the TDOA-based source localization problem consists of finding the corresponding $\mathbf{x}^*$ such that $T_3(\mathbf{x}^*) = (\tau^*_{2,1}, \ldots, \tau^*_{n,1})$. This requires the inversion of T_3.

This map is the focus of the recent extensive analysis of the TDOA system from an algebraic geometry perspective by Compagnoni et al. [12, 13]. The authors specifically consider the two-dimensional TDOA problem as a map as in (2.2). Viewing the problem from this viewpoint allows for the discussion of questions such as: What does the set of feasible TDOA measurements look like? Given a set of TDOA measurements, can we identify the source location they originated from? Is this unique?

In fact, Compagnoni et al. successfully identify the image of T_2 in [12]. This result gave rise to a method for de-noising data developed by the same authors, that involves projecting noisy data onto the image of feasible TDOA measurements [14]. This forces the existence of a real solution $\mathbf{x}^*$ to (2.1). Other methods for managing data to deal with noise include divide and conquer (DAC) and the RANdom SAmpling Consensus method (RANSAC) [16, 17].

In general, source localization using only TDOA measurements is a well-understood problem and many algorithms have been developed for its solution. Common approaches include linearization of the system or a multidimensional parameter search [18]. In 1997, Ho and Chan presented an algorithm that involved reformulating the TDOA equations (2.1) as a system of polynomials, then simplifying to a linear system and a degree 7 polynomial of one variable [8]. Their paper provided a clear introduction to the problem, and its polynomial formulation for the TDOA equations provided a natural starting point for our study of the geolocation problem.

Geometrically, each TDOA measurement restricts the potential transmitter location to a hyperboloid with receivers as the foci (hyperbola in two dimensions). Thus, if several measurements are obtained, locating the emitter requires finding the intersection of several hyperbolae (Figure 2.2). An algebraic closed-form solution to TDOA-based geolocation has been found in several works. Methods for finding these solutions include resultants and Gröbner bases [19, 20], spherical intersection [5, 10], and spherical interpolation [21], among others [6, 22]. Numerical algebraic geometry has also been used for the numerical solution of the TDOA problem in certain applications [23].

2.1.2 Frequency Difference of Arrival (FDOA)

The focus of this dissertation is on the more complicated and less widely studied problem of FDOA-based source localization. While the TDOA is related to the distance between the emitter and the receiver, the FDOA is caused by the Doppler shift of the signal due to disparities between receiver and emitter velocities. With the assumption that the emitter is fixed, the Doppler shift of the signal at receiver i is,

$$d_i = \frac{f_0}{c}\left(\mathbf{v}_i \cdot \frac{\mathbf{x}-\mathbf{x}_i}{\|\mathbf{x}-\mathbf{x}_i\|}\right).$$

This is the dot product of the velocity of the i^{th} receiver ($\mathbf{v}_i = (u_i, v_i, w_i)^T$), with the unit vector pointing from the receiver to the source. This is equivalent to the receiver velocity

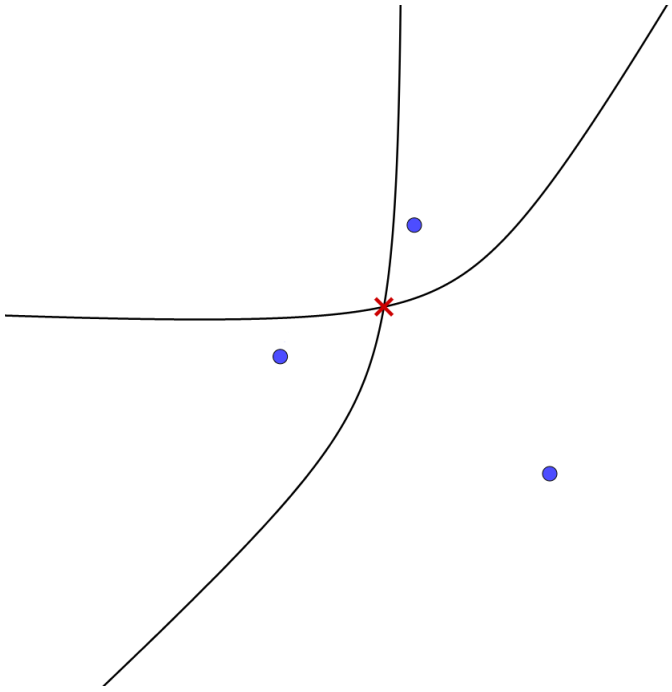

Figure 2.2: Each TDOA measurement restricts the potential transmitter location to a hyperbola. In this figure, receivers are given by blue circles, the resulting curves of potential emitter locations are shown in black, and the emitter location is given by a red X. Note that in three dimensions, the lines of position (LOP) become hyperboloids.

in the direction of the source. The expression is scaled by the center frequency of the transmitted signal (f_0) divided by speed of propagation, c. From here we leave the constant factor $\frac{f_0}{c}$ off for simplicity. This is not an issue as long as f_0 and c are known, which we assume in this thesis. However, in practice, f_0 may be unknown. In this case f_0 could be treated as an additional variable. With the exclusion of the factor $\frac{f_0}{c}$, d_i is *proportional* to the frequency shift of the signal at receiver i. From this we can obtain an expression for the FDOA.

Definition 2. *The* ***frequency difference of arrival (FDOA)*** *between receivers i and 1 is proportional to*

$$f_{1,i} = d_i - d_1 = \mathbf{v}_i \cdot \frac{\mathbf{x} - \mathbf{x}_i}{\|\mathbf{x} - \mathbf{x}_i\|} - \mathbf{v}_1 \cdot \frac{\mathbf{x}_1 - \mathbf{x}}{\|\mathbf{x}_1 - \mathbf{x}\|}. \tag{2.3}$$

As with the TDOA case above, often only the measurements between receivers $2, ..., n$ and receiver 1 are considered and the relationship,

$$f_{i,j} + f_{j,k} - f_{i,k} = 0,$$

holds for noise-free measurements.

Again we consider the receiver positions $\mathbf{x}_1, \ldots, \mathbf{x}_n$ and velocities $\mathbf{v}_1, \ldots, \mathbf{v}_n$ as known parameters and frame the FDOA-based problem (2.3) mathematically as the map:

$$\begin{aligned} F_3 : \ \mathbb{R}^3 &\longrightarrow \mathbb{R}^{n-1} \\ \mathbf{x} &\longrightarrow (f_{1,2}, \ldots, f_{1,n}). \end{aligned} \tag{2.4}$$

FDOA-based source localization then consists of identifying the location $\mathbf{x}^*$ where a signal originated, given that $F_3(\mathbf{x}^*) = (f^*_{1,2}, \ldots, f^*_{1,n})$. There also exists a two-dimensional equivalent of (2.4), F_2. This simpler map is used in Chapter 7. The nonlinear nature of the FDOA equations makes the inversion of F_3 (or F_2) an ill-posed problem, meaning there are multiple solutions. The main approach we use to tackle this difficulty is reformulation of the map F_3 as a system of polynomials. With the receivers' locations and velocities as parameters along with the FDOA measurements, we can solve for the variables corresponding to the source location, $\mathbf{x}$. The solution set of the polynomial system will contain the correct emitter position $\mathbf{x}^*$, along with other points. This approach invites methods from computational and numerical algebraic geometry for the manipulation and solution of polynomial equations.

In the previous section, it was shown that each TDOA measurement limits the possible source locations to a hyperboloid. Unfortunately, the geometric interpretation of the FDOA-based problem is not as simple. Figure 2.3 is an example of the curves of constant FDOA for a fixed set of parameters. Any intersection of the curves in (a) and (b) is a potential emitter location.

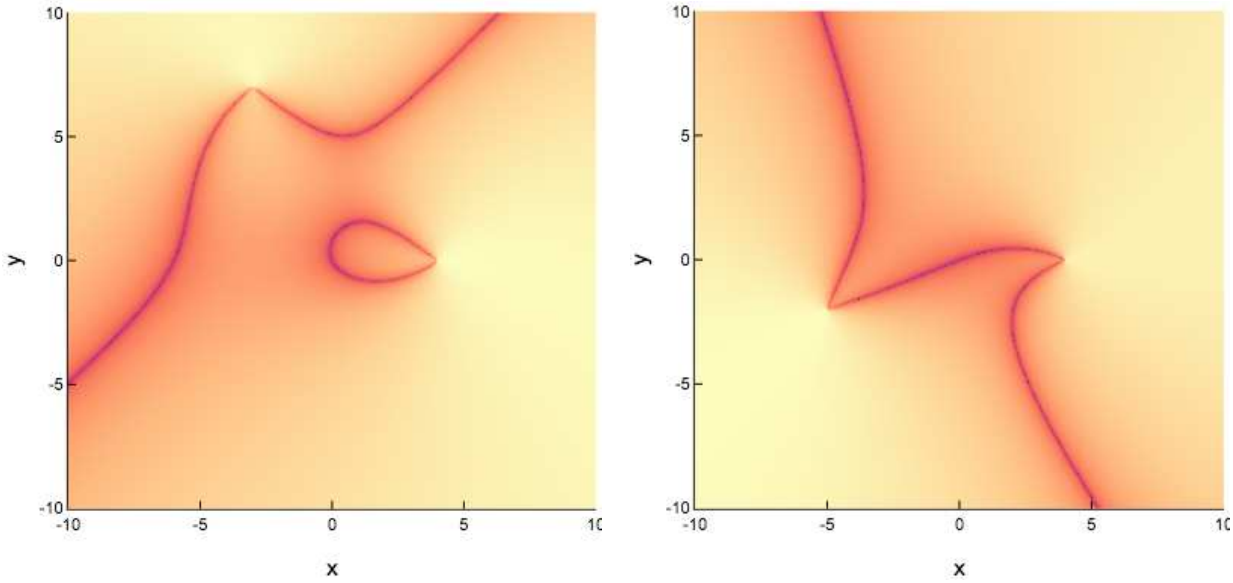

(a) Curve of constant $f_{1,2}$. **(b)** Curve of constant $f_{1,3}$

Figure 2.3: Curves of potential emitter locations resulting from an FDOA measurement. Any point in the intersection of the curves in (a) and (b) is a possible emitter location.

The nonlinearity and corresponding complicated geometry of the FDOA equations make this problem less widely studied than the TDOA case discussed above. While the FDOA measurements are often used as an additional constraint to the TDOA geolocation systems (TDOA/FDOA localization) [8], only a few algorithms have been developed using FDOA alone [24]. In practice, there are some cases where it is desirable to solve for the emitter location using FDOA only. For instance, in the case of a narrowband signal with a long pulse duration, the Doppler resolution is higher than the range resolution and it can be difficult to measure the TDOA accurately [4, 19, 24].

As noted above, the FDOA-based source localization problem is ill-posed. Thus, a few particular issues arise when attempting to find a solution to the problem. The system could have several possible solutions, in which case it can be difficult to distinguish which is correct. Because of this, iterative solvers, such as Newton's method, can converge to a wrong solution. Additionally, small perturbations to the system, i.e., noise, could cause the solutions to become largely inaccurate. Tools from mathematics, such as algebraic geometry,

can provide insight into the behavior of the system. The difficulty and relevance of this problem provide the motivation for this study.

In particular, this dissertation seeks to:

- Express FDOA-based source localization as an algebraic variety. (Chapter 3)
- Develop methods for determining a signal's origin, $\mathbf{x}^*$, when provided with measurements $F_3(\mathbf{x}^*) = (f^*_{1,2}, \ldots, f^*_{1,n})$. These include,
  - A geolocation algorithm combining the iterative method, RANSAC, with numerical algebraic geometry. (Chapter 5)
  - A method for determining the direction of arrival (DOA) of a signal from a set of TDOA or FDOA measurements. (Chapter 6)
- Investigate the geometry of the image of F_3, the set of feasible FDOA measurements. (Chapter 7)

Chapter 3

Polynomial Systems for TDOA and FDOA

It is helpful to transform the TDOA and FDOA equations in Chapter 2 to a set of polynomials. This allows for the use of methods from algebraic geometry. For consistency, the polynomials are presented in three dimensions, although it is easy to see how they could be simplified to a two-dimensional formulation. A polynomial system created from the TDOA equations was used in [8], but the FDOA polynomial expression is new.

3.1 TDOA System

Equation (2.1) can be converted to a polynomial with the use of one additional variable, r_1, to eliminate the square roots. The resulting system is [8]:

$$\begin{aligned}
(c\cdot\tau_{1,2})^2 + 2cr_1\cdot\tau_{1,2} - (x_2^2+y_2^2+z_2^2) + (x_1^2+y_1^2+z_1^2) \\
+ 2\left[(x_2-x_1)x + (y_2-y_1)y + (z_2-z_1)z\right] = 0 \\
(c\cdot\tau_{1,3})^2 + 2cr_1\cdot\tau_{1,3} - (x_3^2+y_3^2+z_3^2) + (x_1^2+y_1^2+z_1^2) \\
+ 2\left[(x_3-x_1)x + (y_3-y_1)y + (z_3-z_1)z\right] = 0 \\
\vdots \\
(c\cdot\tau_{1,N})^2 + 2cr_1\cdot\tau_{1,N} - (x_N^2+y_N^2+z_N^2) + (x_1^2+y_1^2+z_1^2) \\
+ 2\left[(x_N-x_1)x + (y_N-y_1)y + (z_N-z_1)z\right] = 0 \\
r_1^2 - (x^2+y^2+z^2) - (x_1^2+y_1^2+z_1^2) + 2(x_1x + y_1y + z_1z) = 0.
\end{aligned}$$

In addition to its use for removing square roots, r_1 has physical significance as a range variable and represents the distance between the emitter and receiver 1. The variables are emitter location (x, y, z) and range r_1. All other values in the system are parameters. Note that this system is linear except in r_1. This fact was capitalized upon in [8], where the

system was reduced to a single polynomial in r_1. There are well-known methods for solving univariate polynomials, after which the remaining variables can be obtained by a linear solve.

3.2 FDOA System

Similar to the TDOA case above, the FDOA equations can be converted to polynomial equations with the use of several range variables, $r_1, ..., r_N$. Unsurprisingly, this system is more complicated than in the TDOA case.

$$\begin{aligned}
r_1 r_2 f_{1,2} \;-\; & r_1\left[u_2(x_2-x)+v_2(y_2-y)+w_2(z_2-z)\right] \\
& +\; r_2\left[u_1(x_1-x)+v_1(y_1-y)+w_1(z_1-z)\right]=0 \\
r_1 r_3 f_{1,3} \;-\; & r_1\left[u_3(x_3-x)+v_3(y_3-y)+w_3(z_3-z)\right] \\
& +\; r_3\left[u_1(x_1-x)+v_1(y_1-y)+w_1(z_1-z)\right]=0 \\
& \vdots \\
r_1 r_N f_{1,N} \;-\; & r_1\left[u_N(x_N-x)+v_N(y_N-y)+w_N(z_N-z)\right] \\
& +\; r_N\left[u_1(x_1-x)+v_1(y_1-y)+w_1(z_1-z)\right]=0 \\
r_1^2-(x^2+y^2+z^2)-(x_1^2+y_1^2+z_1^2)+2(x_1x+y_1y+z_1z) &= 0 \\
& \vdots \\
r_N^2-(x^2+y^2+z^2)-(x_N^2+y_N^2+z_N^2)+2(x_Nx+y_Ny+z_Nz) &= 0.
\end{aligned}$$

With polynomial representations for the TDOA and FDOA expressions, the geolocation problem is reduced to finding the solution to a set of polynomial equations. The location (x, y, z) and range variables $r_1, r_2, \ldots, r_N$ corresponding to the emitter location will be contained in this solution set. With a problem of this type and size, a solution can be found quickly using techniques from numerical algebraic geometry, particularly with the use of a parameter homotopy (introduced in Section 4.1). Before solving, however, some additional

work must be done to find necessary conditions for a solution to exist and for the solution set to be finite in number.

3.3 Bounds on the Necessary Number of Receivers

For systems of linear equations, it is trivial to predict the dimension of the solution set under the assumption that the equations are linearly independent. This is much the same with polynomial systems, though the range of degenerate cases is far more nuanced and complicated. With the formulation of the geolocation problem as a system of polynomial equations, it is easy to provide bounds on the minimum number of receivers[2] needed in various scenarios to reduce the solution set to a finite set of points. This is the content of Table 3.1. Note that 'TDOA only' refers to solving for location using only TDOA measurements, 'TDOA + FDOA' refers to solving with both TDOA and FDOA, etc.

As an example, we consider the case of solving with only TDOA measurements in three dimensions (x, y, z) using the system in Section 3.1. The number of variables being solved for is four (three location variables and r_1). If there are n receivers, the system above consists of n equations: $n-1$ from TDOA measurements and a single r_1 equation. Solving a single equation in 4 variables results in a three-dimensional solution set. A set with dimension one less than the ambient space is referred to as a *hypersurface*. As the number of non-redundant equations is increased, the dimension of the solution set is typically decreased by one. It follows that a square system (same number of variables and equations) will most-likely result in a zero dimensional solution set (only points). This gives a finite solution set. The number of receivers needed to obtain a square system in the three-dimensional TDOA-only case is $n = 4$. If the emitter's altitude (ALT) is known, the system will have one additional equation and one less receiver is needed to obtain a square system.

[2]If receivers are allowed to take measurements over multiple time steps, the systems would change slightly and a similar table could be provided showing bounds on the number of measurements necessary instead of receivers. This is included in Appendix B.

It is important to note that these bounds do not guarantee that there will be only finitely many solutions for every set of measurements. As an extreme counterexample, consider the case of stacking all receivers at the same point; the number of (identical) measurements in this case makes no difference.

Table 3.1: Minimum number of TDOA and FDOA receivers necessary to reduce set of potential transmitter locations to a finite number, for varying dimensions (2 or 3) and types of measurements being used.

	# receivers (2D)	# receivers (3D)
TDOA only	3	4
TDOA + ALT	-	3
FDOA only	3	4
FDOA + ALT	-	3
TDOA + FDOA	2	3
TDOA + FDOA + ALT	-	2

Chapter 4

Techniques from Algebraic Geometry

In Chapter 3, the TDOA and FDOA expressions (Eqs. 2.1 and 2.3) were converted to polynomial systems with the use of extra variables for removing the square roots. Given parameters and measurement values, the source's location then must lie in the solution set of a system of polynomial equations, referred to as the *algebraic variety* associated with the system. More precisely, the algebraic variety determined by a system of polynomials,

$$F(z) = \begin{pmatrix} f_1(z_1, \ldots, z_N) \\ f_2(z_1, \ldots, z_N) \\ \vdots \\ f_n(z_1, \ldots, z_N) \end{pmatrix},$$

is defined as the set:

$$\mathcal{V}(F) = \{z^* \in \mathbb{C}^N \mid f_i(z^*) = 0 \text{ for all } i\}.$$

In many real-world applications, source-localization included, only the real values of $\mathcal{V}(F)$ are physically realizable. Thus, we wish to consider the *real algebraic variety*, given by $\mathcal{V}(F) \cap \mathbb{R}^N$.

The study of algebraic varieties is precisely the focus of computational algebraic geometry. This work will use both numerical algebraic geometry and symbolic computational algebraic geometry to gain insight into the source localization problem. Numerical algebraic geometry can find all isolated solutions to a system of polynomials with prescribed numerical precision. For example, this field provides methods for solving the FDOA system in Section 3.2. These techniques are presented in Section 4.1. Symbolic methods provide tools for simplifying

systems algebraically and identifying relationships between variables. For this work, we specifically employ tools from elimination theory (Section 4.2).

4.1 Numerical Algebraic Geometry (NAG)

Numerical algebraic geometry provides methods for the numerical solution of polynomial systems using the computational method, *homotopy continuation*. In particular, homotopy continuation can find all finite solutions to a polynomial system. Say there is a *target system*, $F(z)$, to be solved. The process works as follows [15]: First, a simpler system $G(z)$ is constructed; its solutions are known and are referred to as *start points*. Next, a homotopy between the two systems is constructed:

$$H(z,t) = t \cdot G(z) + (1-t) \cdot F(z).$$

When $t = 1$, the solution to $H(z,t) = 0$ is precisely the solution set of $G(z)$, which is known. As t gradually decreases to $t = 0$, the solution to H nears the solution of the target system. The perturbation of t creates paths from the solutions of G to those of F. These paths are followed with numerical predictor-corrector methods, such as Euler's method and Newton's method [25]. Homotopy continuation is implemented in several software programs, including Bertini, Hom4PS, and PHCPack [15, 26, 27]. The work in this dissertation was implemented using Bertini [15].

Homotopy continuation can find all isolated solutions to a system of polynomials with a specified precision. Thus, if parameter values are known, NAG solvers can be used to solve the TDOA/FDOA systems for the location of the emitter. Furthermore, there are a few specialized techniques that can allow for more efficient computation of a solution.

4.1.1 Parameter Homotopy

When performing many solves on a system $F(z;p)$ with the same monomial structure and varying sets of parameters (p), a *parameter homotopy* can be used to speed up compu-

tation [15, 28]. This is useful for the FDOA problem, since the structure of the system is fixed, with only values of $\{\mathbf{x}_1, \ldots, \mathbf{x}_n\}$, $\{\mathbf{v}_1, \ldots, \mathbf{v}_n\}$, and $\{f_{1,2}, \ldots, f_{1,n}\}$ differing between trials. The parameter homotopy consists of two steps. In the first step, the system $F(z; p_0)$ is solved using homotopy continuation, with p_0 a set of random complex numbers. During this step, some paths will usually diverge to infinity. This means that the target system has fewer isolated solutions than the start system. The remaining paths will converge to end points. With probability one, the number of paths tracked to end points in step one is an upper bound for the number of solutions to this system with *any* set of parameter values [15]. Thus, it is only necessary to track this smaller number of paths to solve with the desired set of parameter values p_i. This is the key benefit of a parameter homotopy. In the second step, the end points of $F(z; p_0)$ are used as start points for $F(z; p_i)$, then homotopy continuation is carried out as usual. Note that step one only needs to be completed once per type of system. In this way, solutions can be found for many sets of parameter values relatively quickly.

4.1.2 Singularity

Homotopy continuation consists of many linear solves at every step. Thus one potential issue is for the system to become *singular*. This occurs when paths converge to a multiple root, causing the corresponding Jacobian matrix to drop rank. Over $\mathbb{C}^n$ this is a measure zero event, and theoretically no two paths should converge during homotopy continuation. However, since computation is performed with finite precision, there is a small probability of this happening in reality [15]. Additionally, there is a larger probability that two paths will simply become close or *nearly singular*, causing the problem to become poorly conditioned. To deal with these issues, Bertini utilizes *adaptive precision*, increasing precision when the condition number indicates near-singular behavior. As a trade-off, this can result in slower run-times, but it also allows for accurate path-tracking through troublesome systems.

4.2 Elimination Theory

The area of *elimination theory* provides a framework for manipulating algebraic structures, specifically for the purpose of eliminating variables. This capability can make formulas more useful and computationally accessible, in addition to providing insight into the structure of the problem. Geometrically, eliminating a variable is equivalent to projecting an algebraic variety onto a proper subspace of the original ambient space. In this section we provide a theoretical foundation for elimination methods, then discuss the particular techniques that will be utilized for this work.

4.2.1 Ideals and Varieties

We start by defining a new algebraic object:

Definition 3. *$\mathcal{I} \subset K[z_1, ..., z_n]$ is an **ideal** if:*

1. $\mathbf{0} \in \mathcal{I}$
2. *If $f, g \in \mathcal{I}$ then $f + g \in \mathcal{I}$*
3. *If $f \in \mathcal{I}$ and $h \in K[z_1, ..., z_n]$, then $hf \in \mathcal{I}$. [29]*

Here, $K[z_1, ..., z_n]$ is the *ring* of polynomials with variables $z_1, ..., z_n$ and coefficients in the field K. For our problem, all coefficients are rational, so our ring of interest is $\mathbb{Q}[z_1, ..., z_n]$.

Consider again the system of polynomials,

$$F(z) = \begin{pmatrix} f_1(z_1, \ldots, z_N) \\ f_2(z_1, \ldots, z_N) \\ \vdots \\ f_n(z_1, \ldots, z_N) \end{pmatrix}.$$

The ideal generated by F is denoted $\mathcal{I} = \langle f_1, \ldots, f_n \rangle$ and consists of all polynomial consequences of F. In other words, $\mathcal{I}$ is made up of all polynomial combinations of $f_1, \ldots, f_n$,

$\sum_{i=0}^{n} g_i f_i$ for $g_i \in K[x_1, \ldots, x_n]$, and is the smallest ideal containing F. In the first paragraph of this chapter, the solution set of a system of polynomials was introduced as the algebraic variety, $\mathcal{V}(F)$, associated with the system. In fact, any polynomial in $\mathcal{I} = \langle f_1, \ldots, f_n \rangle$ will vanish on $\mathcal{V}(F)$. Thus,

$$\mathcal{V}(\mathcal{I}) = \{(z_1, \ldots, z_N) \in K^n : f(z) = 0 \text{ for all } f \in \mathcal{I}\}$$

is equivalent to $\mathcal{V}(F)$ [29]. This allows us to consider polynomials in $\mathcal{I}$ other than those explicitly in F for information about the variety of interest.

It is easy to see that every ideal contains an infinite number of polynomials. Thus it is desirable to identify polynomials that lie in $\mathcal{I}$ and possess certain properties. In this chapter, we specifically consider techniques to find polynomials in $\mathcal{I}$ that are lacking particular variables.

4.2.2 Eliminating Variables

Let's start with a basic example of elimination. Consider the ideal,

$$\mathcal{I} = \langle y - (x-2)(x-3),\ y - (x-1) \rangle .$$

The algebraic variety, $\mathcal{V}(\mathcal{I})$, is composed of the points of intersection of the curves:

$$f_1 = y - (x-2)(x+3) = 0$$

and

$$f_2 = y - (x-1) = 0,$$

as shown in Figure 4.1. One way to solve for these points is to manipulate f_1 and f_2 to obtain a polynomial in only one variable. For instance, substituting $y = x - 1$ into f_1 will simplify to the polynomial, $x^2 - 5$. From here, it is easy to see that the x-coordinates of the

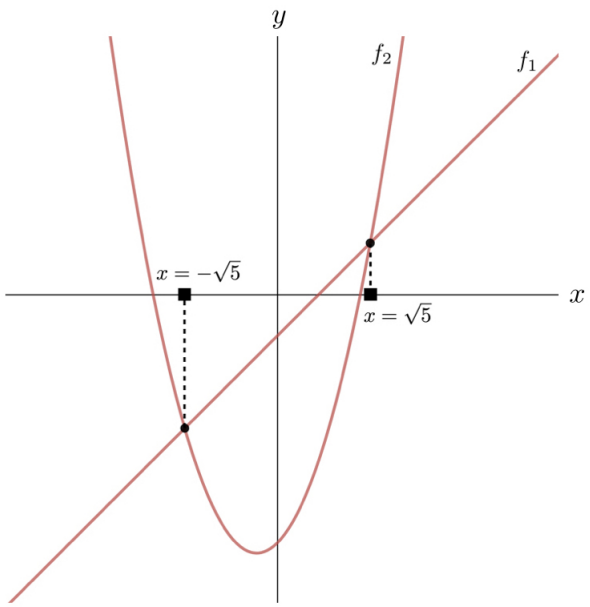

Figure 4.1: Eliminating the variable y from $\langle f_1, f_2 \rangle$ gives the polynomial $x^2 - 5$. This polynomial lies in $\mathcal{I} \cap K[x]$. This variable elimination is essentially equivalent to projecting $\mathcal{V}(\mathcal{I})$ onto the x-axis.

variety are indeed $x = \pm\sqrt{5}$. To find the corresponding y-coordinates of $\mathcal{V}(\mathcal{I})$, the solution $x = \pm\sqrt{5}$ can be *extended* to a solution (x, y) by substituting the x solution into f_1 or f_2.

The ideal, $\mathcal{I} \cap K[x]$, consists of all consequences of $f_1 = 0$ and $f_2 = 0$ which eliminate the y variable. It is referred to as an *elimination ideal*. Since the univariate polynomial $x^2 - 5$ is a polynomial combination of f_1 and f_2 and is only in variable x, it lies in $\mathcal{I} \cap K[x]$. Note that this elimination is essentially equivalent[3] to projecting $\mathcal{V}(\mathcal{I})$ onto its x-coordinate (see Figure 4.1). Elimination allows us to "build up solutions" one coordinate at a time. This is helpful since it is much easier to solve a univariate polynomial than a full system. It also allows for variables that are not of interest to be projected out of the system.

4.2.3 Resultants

The elimination technique that proved most useful for this project is the computation of resultants. Given two polynomials, resultants provide a way of determining whether the two

[3]In general, the projection of $\mathcal{V}(\mathcal{I})$ onto a subset of coordinates, e.g.,$x_l, \ldots, x_k$, is *contained* in $\mathcal{I} \cap K[x_l, ..., x_k]$ and the ideal may contain some extraneous algebraic components. For the sake of relevance, this is not discussed here. See Chapter 3 of [29] for more information.

polynomials share a common factor. This is equivalent to determining whether the polynomials share a root in $\mathbb{C}$ [29]. Elimination with resultants avoids factoring the polynomials or performing polynomial division, both of which can be computationally expensive.

We begin by stating a result that lays the foundation for resultant computation. The univariate case is considered for simplicity. We will explore how this can be extended to the multivariate case later.

Theorem 4. *Consider two polynomials, f and g, with degrees l and m, respectively. The polynomials have a common factor if and only if there exist polynomials A and B with degrees less than m and l, respectively, such that,*

$$Af + Bg = 0,$$

where at least one of A and B is nonzero. [29]

Now, it can be expensive to find A and B explicitly, but we can focus instead on finding conditions for an appropriate A and B to exist. Say the polynomials f and g are given by:

$$f = c_0 + c_1 x + \ldots + c_l x^l$$
$$g = d_0 + d_1 x + \ldots + d_m x^m.$$

If A and B exist, they will have the form:

$$A = a_0 + a_1 x + \ldots + a_{m-1} x^{m-1}$$
$$B = b_0 + b_1 x + \ldots + b_{l-1} x^{l-1}.$$

Substituting these polynomials into $Af + Bg = 0$ and setting coefficients equal to zero, we get the system:

$$
\begin{aligned}
a_0c_0 &+ b_0d_0 &&= 0\\
a_0c_1 + a_1c_0 &+ b_0d_1 + b_1d_0 &&= 0\\
\ddots &\qquad\ddots &&\vdots\\
a_{m-1}c_l &+ b_{l-1}d_m &&= 0.
\end{aligned}
$$

This forms a linear system in the variables $a_0,\ a_1,\ \ldots,\ a_{m-1}$ and $b_0,\ b_1,\ \ldots,\ b_{l-1}$. If there exists a nontrivial solution to this system, then there exist an A and B such that the condition in Theorem 4 is satisfied. We can represent this system with the matrix of coefficients,

$$
\mathrm{Syl}(f,g;x) = \begin{bmatrix}
c_0 & & & d_0 & & \\
c_1 & c_0 & & d_1 & d_0 & \\
 & \ddots & & & \ddots & \\
 & & c_l & & & d_m
\end{bmatrix},
$$

referred to as the *Sylvester matrix* [29]. Thus, we would like to know if there is a nontrivial solution to:

$$
\mathrm{Syl}(f,g;x) \cdot \begin{bmatrix} a_0 \\ \vdots \\ a_{m-1} \\ b_0 \\ \vdots \\ b_{l-1} \end{bmatrix} = \begin{bmatrix} 0 \\ \vdots \\ \\ \\ \vdots \\ 0 \end{bmatrix}.
$$

This occurs precisely when the determinant of the Sylvester matrix is equal to zero. Thus, the resultant is defined as [29],

$$\mathrm{Res}(f, g; x) = \det(\mathrm{Syl}(f, g; x)).$$

Furthermore, f and g have a common factor precisely when $\mathrm{Res}(f, g; x) = 0$.

The following example shows how this tool is useful for elimination of variables.

Example 5. *Consider again the ideal from Section 4.2.2:*

$$\mathcal{I} = \langle y - (x-2)(x+3),\ y - (x-1)\rangle = \left\langle y - x^2 - x + 6,\ y - x + 1\right\rangle.$$

The expressions f_1 and f_2 are multivariate with variables x and y. We would like to eliminate y by finding a polynomial in $\mathcal{I} \cap K[x]$. Thus, we compute the resultant with respect to variable y,

$$\begin{aligned}\mathrm{Res}(f_1, f_2; y) &= \begin{vmatrix} -x^2 - x + 6 & -x + 1 \\ 1 & 1 \end{vmatrix} \\ &= (-x^2 - x + 6) - (-x - 1) \\ &= -x^2 + 5.\end{aligned}$$

Notice that the coefficients of y are polynomials in x. Thus, the resultant ends up being a polynomial in x. Furthermore, $-x^2 + 5 \in \mathcal{I} \cap K[x]$.

Thus, resultants provide a systematic way to find polynomials in the elimination ideal. The resultant introduced above is specifically referred to as the *Sylvester resultant*. There are also methods for resultants involving more than two polynomials, called *multipolynomial resultants*. In particular, we find the *Dixon resultant* to be useful for this work for the sake of fast computation [30]. This will be covered in more detail when the Doppler shift surface is introduced in Chapter 7.

Chapter 5

Numerical Algebraic Geometry and RANSAC for FDOA-based Geolocation

This chapter describes a novel geolocation algorithm that combines the solving power of numerical algebraic geometry with the robustness to noise of the RANdom SAmpling Consensus method. This project was presented at IEEE Radar Conference 2018 and has been published in the conference proceedings [31].

5.1 Motivation and Overview

With a noiseless system, numerical algebraic geometry (NAG) methods can be used to find all solutions to the FDOA system presented in Section 3.2 accurate to any prescribed numerical accuracy. Specifically, it would take only a single solve in a NAG software such as Bertini [15] to obtain an emitter location. However, there are a couple issues that arise in real world situations. First, noise and measurement error can plague FDOA calculations and receiver location and velocity estimates. Additionally, if the receivers are positioned in a singular configuration or near one, computing the solution may be prohibitively expensive and the solution itself could be much more accurate in some coordinates than in others. The nonlinear nature of the problem implies that there will often be multiple real solutions, which translate to multiple potential emitter locations. A robust accompaniment for the numerical algebraic geometry methods is an iterative process such as the RANdom SAmple Consensus (RANSAC) algorithm.

The proposed algorithm has two main components: numerical solution of the FDOA polynomial system using the NAG software, Bertini [15], and comparison of solutions with RANSAC. An overview of numerical algebraic geometry methods is provided in the previous chapter. This chapter will then begin with an overview of the RANSAC algorithm as it

is to be used in this project (Section 5.2). Section 5.3 then introduces a novel bound for FDOA measurements that allows for data with high amounts of noise to be thrown out immediately. The proposed geolocation algorithm using both NAG and RANSAC is presented with numerical results in Section 5.4 . The chapter ends with a discussion of limitations and benefits of the method (Section 5.5).

5.2 RANdom SAmpling Consensus (RANSAC) Method

RANSAC, originally developed [32] for application to the location determination problem, is useful when one has data with outliers or corrupt data points. The algorithm works by choosing a few samples from a set of data, determining a model to fit the samples, then calculating how many of the remaining data points can be considered inliers with respect to that model, up to a predetermined tolerance. This process is repeated for a prescribed number of iterations, then the model with the most inliers is returned.

Using RANSAC for geolocation is not a new idea. In fact, Li et al. applied the algorithm to source location with TDOA in [17]. This paper proposes a modification of RANSAC to solve for source location with the FDOA polynomial system, a problem that is now accessible due to the utilization of numerical algebraic geometry techniques.

The most notable benefit of using RANSAC for this problem is the ability to “ignore" noisy or corrupt data. Additionally, since many FDOA measurements are needed for the algorithm, it is natural to reformulate the polynomial system presented in Section 3.2 to allow for measurements to be taken over multiple time steps. This reduces the number of receivers needed to a single pair, with each system composed of FDOA measurements from three separate time steps[4].

[4]See Appendix B for more information on the system reformulation.

5.3 Note on Denoising

Since one of the key contributions of this project is the use of RANSAC for denoising data, we include here a brief result that allows us to immediately remove FDOA measurements that are physically unrealizable due to measurement error or noise.

Proposition 6. *The frequency difference of arrival between receivers i and j, $f_{i,j}$ satisfies:*

$$|f_{i,j}| \leq \frac{f_0}{c} \left(\|\mathbf{v}_j\| + \|\mathbf{v}_i\| \right),$$

where $\mathbf{v}_i$ and $\mathbf{v}_j$ are the velocity vectors of receivers i and j, respectively.

Proof.

$$\begin{aligned}
|f_{i,j}| &= \frac{f_0}{c} \left| \frac{\mathbf{v}_j \cdot (\mathbf{x}_j - \mathbf{x})}{\|\mathbf{x}_j - \mathbf{x}\|} - \frac{\mathbf{v}_i \cdot (\mathbf{x}_i - \mathbf{x})}{\|\mathbf{x}_i - \mathbf{x}\|} \right| \\
&= \frac{f_0}{c} \left| \frac{\|\mathbf{v}_j\| \|\mathbf{x}_j - \mathbf{x}\| \cos(\theta_j)}{\|\mathbf{x}_j - \mathbf{x}\|} - \frac{\|\mathbf{v}_i\| \|\mathbf{x}_i - \mathbf{x}\| \cos(\theta_i)}{\|\mathbf{x}_i - \mathbf{x}\|} \right| \\
&= \frac{f_0}{c} \left| \|\mathbf{v}_j\| \cos(\theta_j) - \|\mathbf{v}_i\| \cos(\theta_i) \right| \\
&\leq \frac{f_0}{c} \left(\|\mathbf{v}_j\| + \|\mathbf{v}_i\| \right).
\end{aligned}$$

□

5.4 FDOA-RANSAC (FDOAR) Algorithm

The proposed algorithm considers measurements from a single pair of receivers at n time steps. After removing points with obvious corruption (according to Prop. 6), subsets of three time steps[5] are randomly chosen from the set of measurements. This data is used to construct a polynomial system. The system is similar to that given in Chapter 3, but since we are now considering a single pair of receivers over multiple time steps, it changes slightly.

[5]See Table B.1 for why three time steps are needed.

See Appendix B for more information. The system is then solved using Bertini [15]. The solutions found with Bertini are then fed through the forward map and RANSAC is used to determine which solution fits the remaining data best. This process is iterated over different choices of measurement subsets. See pseudocode for this method in Algorithm 1.

The algorithm involves solving a system using the numerical algebraic geometry software, Bertini [15], during each iteration. Since each system will be of the same form and change only in certain parameter values (location, velocity, FDOA measurements), the solve can be structured as a parameter homotopy [15, 28]. As discussed in Section 4.1, this allows for only necessary paths to be tracked, which provides faster run times. Additionally, when the solving of an FDOA system results in multiple real, feasible solutions, we have modified the algorithm to consider each solution separately. This ensures there are no missed solutions, as can often result from iterative geolocation methods that converge to a single solution [19].

5.4.1 Numerical Performance

Numerical simulations were run as follows. Consider a Cartesian cube of space, 100m long on each side. These lengths were chosen arbitrarily and can be scaled. For each numerical trial, a transmitter was placed at a random location, $\mathbf{x}$, in the cube. Locations and velocities for 40 pairs of receivers were also generated, with locations being limited to the interior of the cube and velocities in the range $[-2, 2]$ m/s in each (x,y,z) direction. This is meant to simulate 40 time steps for a single pair of receivers and a stationary transmitter. For each pair of receivers, the FDOA was calculated according to (2.3) and noise was added to simulate various levels of relative FDOA measurement error. We define this,

$$\text{Relative FDOA Measurement Error } := \frac{\sigma^2_{noise}}{\sigma^2_{FDOA}} \times 100\%,$$

where σ^2_{noise} and σ^2_{FDOA} are the variance of the noise and variance of observed FDOA, respectively. The FDOAR algorithm was then run for 20 iterations, returning final transmitter estimate $\hat{\mathbf{x}}$. The error for the trial was then calculated: $\|\hat{\mathbf{x}} - \mathbf{x}\|$ (m). Results are shown

Algorithm 1 RANSAC for transmitter location with FDOA measurements.
Input: Locations, velocities, and corresponding FDOA measurement(f_i) for 1 pair of receivers at n time steps; number of iterations to run algorithm ($numiter$), inlier tolerance (ε).
Output: Estimated transmitter location, $\hat{\mathbf{x}}$.

Set $trial = 0$
while $trial < numiter$ **do**
    Select 3 sample points (between 1 and n) from receiver data (FDOA measurements, receiver locations, and receiver velocities).
    Solve for location by running system[6] in Bertini [28].
    Record feasible solutions, $sols$. ▷ Solutions must have feasible range values and satisfy Prop. 6.
    for ℓ in $sols$ **do**
        $numinliers = 0$ ▷ Counts inliers for solution.
        for {each pair of receivers: k}\{pairs in sample} **do**
            Calculate theoretical FDOA meas. for solution ℓ and pair of receivers k.
            if |Actual FDOA - Est. FDOA| $< \varepsilon$ **then**
                Increment $numinliers$.
            end if
        end for
        if $numinliers > bestmodel$ **then**
            $bestmodel = numinliers$
            Record location as new best transmitter location estimate.
        end if
    end for
    Increment $trial$.
end while
return $\hat{\mathbf{x}}$.

in Figure 5.1. For each data point, this process was repeated 50 times and the median of the error was recorded. Other metrics, such as MSE, could also be used, but median was chosen for its robustness to outliers.

Many of the worst performing trials above resulted from transmitters located near the edges of the Cartesian box. We hypothesize that this is the result of very few (or none) of the receiver pairs being located on the side of the transmitter closest to the edge of the box. This caused less information to be learned about the transmitter and resulted in a worse estimate. This is consistent with geolocation intuition and suggests that error values in Fig. 5.1 would decrease if one could ensure that receivers view the emitter from a variety of angles.

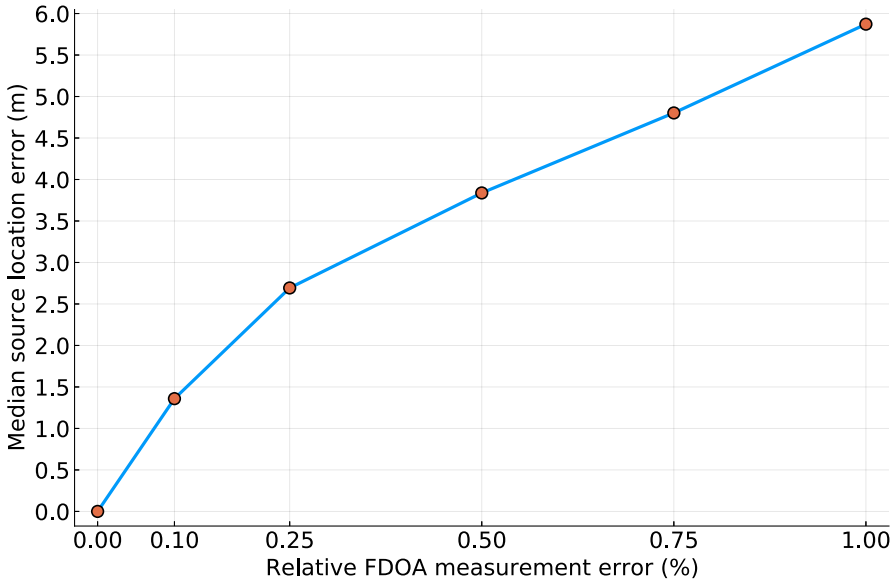

Figure 5.1: Error in emitter location resulting from various levels of FDOA measurement error. For each data point, 50 instances of coupled RANSAC and Bertini were run, each having 20 iterations and $\varepsilon = 0.03$.

5.5 Discussion

5.5.1 Benefits of FDOAR

We summarize a few of the primary benefits of our approach here:

1. Solving the geolocation systems using numerical algebraic geometry techniques finds all possible emitter locations. Coupling with RANSAC provides a way to determine which one of those locations best matches the rest of the data.

2. Any bad data from path failures, inaccuracies, measurement error, etc. is automatically ignored, assuming the source of the errors is not implicit in the structure of the problem.

3. This method uses FDOA measurements only, though it can be adapted to other measurement combinations.

4. Using multiple time steps, it is necessary to use only two receivers. Additionally, there is no need to designate a reference receiver, which could corrupt all data points if there are errors in its location or velocity.

5. When performing polynomial system solves at multiple points in parameter space, parameter homotopies could improve efficiency.

5.5.2 Limitations

Each path tracked when solving a polynomial system requires dozens, sometimes hundreds, of linear solves. As a result, any polynomial systems approach will necessarily be slower than any linear approach. However, linearization necessarily introduces inaccuracy to nonlinear problems, so the trade-off between speed and accuracy might lead different users to use different approaches.

As with any RANSAC implementation, speed and accuracy is in part dependent upon the users choice of the maximum number of iterations and inlier tolerance. The optimal choice for these variables can depend greatly on the specifics of the problem. Theoretical results exist that bound the maximum number of iterations with respect to the percentage of inliers present in the data [33].

Chapter 6

Determining Direction of Arrival from Far-Field TDOA or FDOA Measurements

Thus far, this research has focused primarily on source localization with TDOA and FDOA measurements. Another useful quantity for describing the location of an emitter is the *angle of arrival* (AOA) of a signal, also referred to as the *direction of arrival* (DOA). This chapter explores the interesting relationship between these quantities, especially when working in the *far-field*. This leads to a novel method for determining direction of arrival from FDOA or TDOA measurements. This chapter corresponds to a stand-alone paper that will be submitted for publication [34].

6.1 Introduction

When using a single antenna array, simple geometric relationships between the TDOA measurements and the known receiver positions allow the direction of arrival to be computed through a process known as phase interferometry [35]. It follows that with multiple antenna arrays, the source can be located via triangulation. No analogous method exists using FDOA measurements. Other techniques for determining the direction of arrival of a signal include the use of rotating directional antennas or Doppler direction finders [36]. The latter of these utilizes the Doppler effect, although with a rather different approach than FDOA.

When the distance between the receivers and the transmitter is much greater than the distance between the receivers it is common to simplify the wave propagation model and assume that wave curvature is negligible in the region of the receivers. This assumption is commonly referred to as the far-field assumption [4]. In this paper we present how this assumption can reduce the computation of DOA to the solution of a linear system.

While DOA estimation is typically performed with a TDOA-based strategy, our approach is able to utilize TDOA or FDOA measurements, perhaps both, by capitalizing on the simplified geometry of the source-localization problem under the far-field assumption. One scenario where this method might be useful is in the calculation of DOA of a narrowband emitter using several receivers. The main benefit of this method is its computational efficiency, as it simplifies the calculation of DOA to solving a linear system of equations. With several DOA calculations, triangulation can be used to determine location of the source. In Section 6.2, we develop a far-field model for the FDOA measurements and discuss a technique for determining the signal direction of arrival.

This chapter is structured as follows. In Section 6.3, we develop a similar far-field approximation for the TDOA model and present the analogous DOA technique. Finally, we summarize the method with some numerical results in Section 6.4 and concluding remarks in Section 6.5.

6.2 Direction of Arrival with FDOA Measurements

Consider a stationary transmitter located at $\mathbf{x}$. Suppose we have n receivers located at $\mathbf{x}_1, ..., \mathbf{x}_n$ with velocities $\mathbf{v}_1, ..., \mathbf{v}_n$. As presented in Chapter 2, the frequency shift of the signal between the emitter and the i^{th} receiver is

$$d_i = \frac{f_0}{c}\left(\mathbf{v}_i^T \cdot \frac{\mathbf{x}_i - \mathbf{x}}{\|\mathbf{x}_i - \mathbf{x}\|}\right), \tag{6.1}$$

where f_0 is the center frequency of the emitter and c is the speed of wave propagation in the media. In our scenario, we know the receiver positions and velocities, and we would like to solve for the transmitter position. We cannot measure the frequency shift directly, but we can measure the difference in frequency shifts, $f_{i,j} = d_j - d_i$. Scaling by $\|\mathbf{x}_i - \mathbf{x}\|^{-1}$ means that each of these equations is nonlinear. Even so, by taking pairwise differences of the equations in (6.1), one can numerically solve the system by expressing it in terms of

polynomials and using techniques like homotopy continuation, as discussed in Chapter 5 [31]. While such an approach is able to find all solutions, it is computationally more expensive than a linear solve.

The nonlinearity of (6.1) makes it difficult to accurately solve for $\mathbf{x}$, so we simplify the model by deriving a far-field approximation for Equation 6.1. Additionally, for simplicity we ignore the constant factor of f_0/c in (6.1). Thus d_i is now *proportional* to the frequency shift.

6.2.1 Far-field Approximation for FDOA

Assume without loss of generality that the receivers are centered around the origin. We consider the far-field case, where the distance between receivers is much smaller than the distance to the emitter, i.e. $\|\mathbf{x} - \mathbf{x}_i\| >> \|\mathbf{x}_i\|,\ \forall\ i$. The far-field approximation (as in [4]) for $1/\|\mathbf{x} - \mathbf{x_i}\|$ is:

$$\frac{1}{\|\mathbf{x} - \mathbf{x_i}\|} = \frac{1}{\|\mathbf{x}\|}\left(1 + \mathcal{O}\left(\frac{\|\mathbf{x}_i\|}{\|\mathbf{x}\|}\right)\right).$$

Truncating after the first term above allows for simplification of the factor (in Eq. 6.1):

$$\frac{\mathbf{x}_i - \mathbf{x}}{\|\mathbf{x}_i - \mathbf{x}\|} \approx \frac{\mathbf{x}_i}{\|\mathbf{x}\|} - \frac{\mathbf{x}}{\|\mathbf{x}\|}.$$

Additionally, the far-field assumption implies that the first term will have small magnitude. Thus, $\dfrac{\mathbf{x_i} - \mathbf{x}}{\|\mathbf{x_i} - \mathbf{x}\|}$ is simplified to $\dfrac{-\mathbf{x}}{\|\mathbf{x}\|}$. Equation 6.1 becomes:

$$d_i = -\mathbf{v}_i^T \hat{\mathbf{x}}, \tag{6.2}$$

where $\hat{\mathbf{x}} = \frac{\mathbf{x}}{\|\mathbf{x}\|}$, is the unit vector in the direction of $\mathbf{x}$. The entire system of frequency shifts can be written:

$$\mathbf{d} = -\mathbf{V}\hat{\mathbf{x}}, \tag{6.3}$$

where

$$\mathbf{d} = \begin{pmatrix} d_1 \\ \vdots \\ d_n \end{pmatrix} \qquad \mathbf{V} = \begin{pmatrix} \mathbf{v}_1^T \\ \vdots \\ \mathbf{v}_n^T \end{pmatrix}.$$

In practice, the frequency shifts are not observable. Instead the frequency difference of arrival (FDOA) is measured between receivers. The FDOA is equivalent to the difference in frequency shifts,

$$f_{i,j} = d_j - d_i. \tag{6.4}$$

A system equivalent to (6.3) can be constructed for the FDOA, with the use of a differencing matrix $\mathbf{P}$. The matrix $\mathbf{P}$ has entries of 0 and ± 1 corresponding to the differencing in (6.4). For instance, we can represent the measurements $(f_{1,2}, f_{1,3})$ as

$$\begin{pmatrix} f_{1,2} \\ f_{1,3} \end{pmatrix} = \begin{pmatrix} -1 & 1 & 0 \\ -1 & 0 & 1 \end{pmatrix} \begin{pmatrix} d_1 \\ d_2 \\ d_3 \end{pmatrix} = \mathbf{P}\mathbf{d}.$$

Thus, with the far-field simplification above, the vector of FDOA measurements, $\mathbf{f}$, is equivalent to,

$$\mathbf{f} = -\mathbf{P}\mathbf{V}\hat{\mathbf{x}}. \tag{6.5}$$

The matrix $-\mathbf{P}\mathbf{V}$ will be referred to as $\widetilde{\mathbf{V}}$ for simplicity.

This far-field simplification reduces the FDOA equations to a linear system. This suggests that FDOA measurements in the far-field case lie on the image of the unit circle transformed by the matrix $\widetilde{\mathbf{V}}$. This image is an ellipse with rotation and scaling detectable from the singular value decomposition of $\widetilde{\mathbf{V}}$. Indeed, this can be confirmed by computing the singular value decomposition of generated far-field FDOA measurements and confirming they lie on the same subspace as $\widetilde{\mathbf{V}}$. This relationship can be demonstrated visually with a plot of generated FDOA measurements (Fig. 6.1).

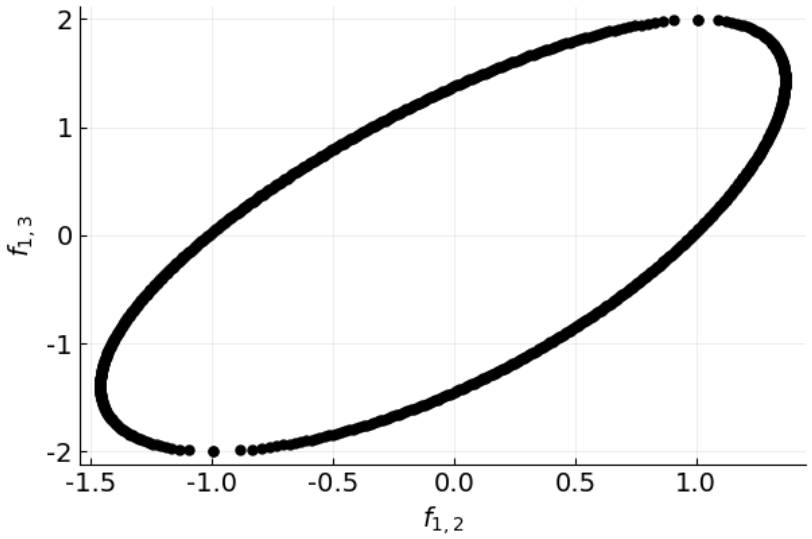

Figure 6.1: Plot of far-field $f_{1,2}$ vs. $f_{1,3}$ for a system of three receivers centered around the origin. Note the image is an ellipse with scaling in the direction of the left singular vectors of $\widetilde{\mathbf{V}}$.

6.2.2 Calculating direction of arrival (DOA)

The far-field approximated form of the FDOA equations is linear with variable $\hat{\mathbf{x}}$, representing the direction of arrival (DOA) of the signal. Thus, the DOA can be found by solving (6.5) for $\hat{\mathbf{x}}$. If there are more FDOA measurements than direction components, we can find the least squares solution to the problem, which is also the pseudo-inverse solution:

$$\hat{\mathbf{x}} = (\widetilde{\mathbf{V}}^T\widetilde{\mathbf{V}})^{-1}\widetilde{\mathbf{V}}^T\mathbf{f}. \tag{6.6}$$

It is necessary that the matrix $\widetilde{\mathbf{V}}$ be nonsingular for a solution to exist to (6.6). This adds a requirement that the relative velocities of the receivers are nonzero.

One method for de-noising in TDOA-based geolocation is the projection of noisy measurements onto the range of the differencing matrix $\mathbf{P}$ [7, 14]. This ensures that the TDOA measurements are physically realizable and consistent between receivers by enforcing a closed loop condition. One benefit of the method for DOA calculation proposed above is that de-noising is automatically performed since projection onto the range of $-\mathbf{PV}$ is equivalent to projection onto the range of $\mathbf{P}$. In Chapter 7 we explore this de-noising method further and discuss additional algebraic conditions that FDOA measurements must satisfy.

6.3 Direction of Arrival with TDOA Measurements

Although the time difference of arrival (TDOA) is simpler than the FDOA case, we include its far-field approximation for completeness. This leads to a method for determining DOA with TDOA measurements that is analogous to the relationship developed in the previous section.

Using the same problem setup as above, the time it takes for the signal to travel between the emitter and receiver i is:

$$\tau_i = \frac{1}{c}\|\mathbf{x_i} - \mathbf{x}\|,$$

from here the scalar $\frac{1}{c}$ will be left out for simplicity. The far-field approximation for $\|\mathbf{x_i} - \mathbf{x}\|$ is given [4],

$$\|\mathbf{x_i} - \mathbf{x}\| = \|\mathbf{x}\| \left(1 - \frac{\mathbf{x}_i \cdot \hat{\mathbf{x}}}{\|\mathbf{x}\|} + \mathcal{O}\left(\frac{\|\mathbf{x}_i\|}{\|\mathbf{x}\|}\right)\right).$$

Thus, τ_i becomes

$$\tau_i = \|\mathbf{x}\| - \mathbf{x}_i \cdot \hat{\mathbf{x}}.$$

As in the FDOA case, τ_i is not observable. Instead we look to the time difference of arrival (TDOA) between receivers i and j,

$$\begin{aligned}\tau_{i,j} &= (\|\mathbf{x}\| - \mathbf{x}_j \cdot \hat{\mathbf{x}}) - (\|\mathbf{x}\| - \mathbf{x}_i \cdot \hat{\mathbf{x}}) \\ &= \mathbf{x}_i \cdot \hat{\mathbf{x}} - \mathbf{x}_j \cdot \hat{\mathbf{x}} \\ &= (\mathbf{x}_i - \mathbf{x}_j) \cdot \hat{\mathbf{x}}.\end{aligned}$$

The system of TDOA measurements are equivalent to

$$\boldsymbol{\tau} = -\mathbf{P}\mathbf{X}\hat{\mathbf{x}}, \tag{6.7}$$

where $\mathbf{X}$ is the matrix of receiver locations and $\mathbf{P}$ is a differencing matrix as before. This suggests that feasible far-field TDOA measurements lie in the image of the unit circle under transformation of $-\mathbf{PX}$.

As in the FDOA case, the least-squares estimate of direction of arrival can be calculated using the pseudoinverse:

$$\hat{\mathbf{x}} = -((\mathbf{PX})^T\mathbf{PX})^{-1}(\mathbf{PX})^T\tau. \tag{6.8}$$

6.4 Numerical Results

One method of estimator evaluation is the comparison of estimator variance with the Cramer Rao lower bound (CRLB). Assuming data with additive noise distributed Gaussian with a given covariance matrix, the CRLB provides a lower bound on the variance of estimator accuracy. We consider here the FDOA-based DOA estimation problem. Consider FDOA measurements, $\hat{f}_{ij}$, equal to the sum of the true FDOA and Gaussian-distributed deviation. That is,

$$\hat{\mathbf{f}} = \mathbf{f} + \delta\mathbf{f},$$

where $E[\delta\mathbf{f}] = 0$ and $E\left[\delta\mathbf{f}\delta\mathbf{f}^T\right] = \mathbf{Q}$. The CRLB can then be computed for data with noise corresponding to covariance matrix $\mathbf{Q}$. This provides a lower bound on variance of DOA estimation using FDOA measurements. It follows that an algorithm with variance near the CRLB has optimal accuracy with the given level of noise. For ease of visualization, we will consider the CRLB corresponding to the AOA (given by θ) as opposed to DOA.

The CRLB of an unbiased estimator is the inverse of the Fisher information matrix, $\mathbf{J}$. For the FDOA based AOA problem, this is given by [8]:

$$\mathbf{J}(\mathbf{x}, \mathbf{X}, \mathbf{V}; \mathbf{Q}) = \left(\frac{\partial \mathbf{f}^T}{\partial \mathbf{x}} \cdot \frac{\partial \mathbf{x}}{\partial \theta}\right) \mathbf{Q}^{-1} \left(\frac{\partial \mathbf{f}}{\partial \mathbf{x}^T} \cdot \frac{\partial \mathbf{x}^T}{\partial \theta}\right).$$

This can be calculated for a fixed set of receiver positions ($\mathbf{X}$), velocities ($\mathbf{V}$), covariance matrix ($\mathbf{Q}$), and emitter location ($\mathbf{x}$). The result is a single value whose inverse is the CRLB for AOA.

Numerical trials can then be run with our DOA approximation method and the variance in DOA can be compared to the CRLB. Figure 6.2 shows this comparison for a four receiver configuration shown in Figure 6.3. The covariance matrix used for this simulation was

$$\mathbf{Q} = c^2\sigma^2 \begin{bmatrix} 1 & 0.5 & \dots & 0.5 \\ 0.5 & \ddots & 0.5 & \vdots \\ \vdots & 0.5 & \ddots & 0.5 \\ 0.5 & \dots & 0.5 & 1 \end{bmatrix},$$

where σ^2 is the FDOA variance. This choice of $\mathbf{Q}$ is chosen to be consistent with similar numerical trials in [8]. The dimensions of $\mathbf{Q}$ are 6×6 since 4 receivers result in $\binom{4}{2}$ FDOA measurements. We define noise power as $c\sigma$.

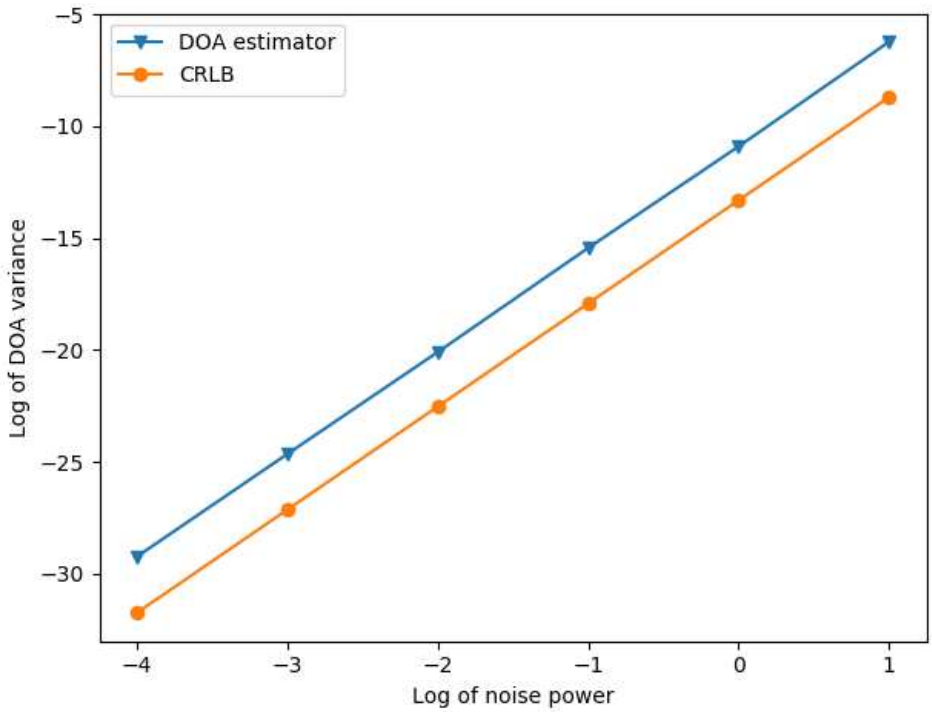

Figure 6.2: Log-log plot of DOA estimator error vs. the Cramer Rao lower bound on FDOA-based DOA variance for receivers with configuration shown in Figure 6.3.

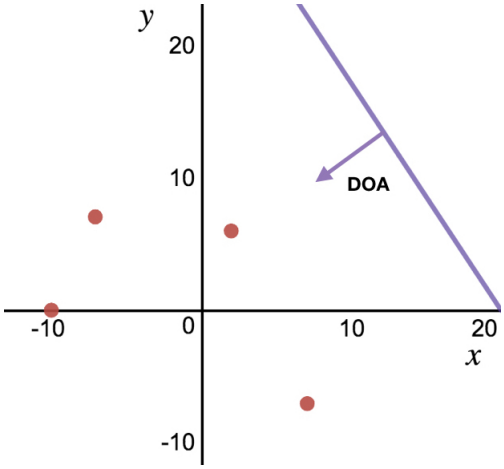

Figure 6.3: Receiver configuration for CRB comparison in Figure 6.2.

The x-axis of Figure 6.2 gives varying levels of noise power and the y-axis shows corresponding AOA variance for our approximation and the CRLB. It is clear that the AOA variance trend mimics that of the CRLB, but is consistently above it.

6.5 Conclusion

Considering far-field FDOA-based geolocation naturally leads to a simple method for determining direction of arrival. This calculation requires only a linear solve which makes the corresponding source-localization technique very efficient. Additionally, since FDOA measurement data is projected onto the range of the differencing matrix, the solution is naturally de-noised in a method consistent with [7, 14]. Another benefit of this method is the generality that allows DOA to be calculated with either TDOA or FDOA measurements. This allows for accurate source localization in the presence of a range of waveforms.

Chapter 7

The Surface of Feasible Doppler Shifts

In real-world source-localization scenarios, signals may be corrupted by noise or measurement error. This can result in a set of measurements that, when taken together, correspond to no real source location. Thus, we are motivated to identify the set of feasible FDOA measurements given by the *image* of the FDOA map introduced in Chapter 2. This is done using some of the algebraic geometry techniques discussed in Chapter 4. Utilizing resultants (Section 4.2.3), we are able to find an algebraic expression that every set of Doppler shifts for a given scenario must satisfy. This could be useful for the de-noising of FDOA measurements.

7.1 Motivation

In [12–14], Compagnoni et al. perform a comprehensive analysis of range maps, specifically focusing on the TDOA map. They show that the image of a range map forms an algebraic surface, specifically classified as a Kummer surface[7] [13]. Since the TDOA map is given by the differencing of ranges, the image of the TDOA map is then a projection of this surface. Compagnoni et al. identify the set of feasible TDOA measurements, or the image of the map T_2 that was introduced in Section 2.1.1, as the convex bounded region in $\mathbb{R}^2$ corresponding to the projection of the range map surface.

In [14], identifying this set is shown to be useful for de-noising of TDOA measurements. Essentially, the distance between raw TDOA measurements and the bounded region of feasible TDOA is minimized, resulting in a feasible and de-noised set of TDOA measurements. This is shown to improve the performance of TDOA-based source localization algorithms [14].

[7] A Kummer surface is defined by a polynomial of degree 4 with 16 isolated singular points [13].

In this chapter, we aim to identify an algebraic expression for the set of feasible Doppler shifts and corresponding FDOA measurements. This can then be compared to the range map surface and set of feasible TDOA measurements. Exploring the Doppler shift surface further will help us to evaluate the possibility for an FDOA de-noising technique analogous to that developed in [14].

Investigating the set of feasible Doppler shifts involves the use of elimination theory and resultants. We specifically find the Dixon resultant, a type of multivariate resultant, to be useful and computationally efficient for eliminating variables. The use of multivariate resultants as a means of solving the source localization problem has been explored in [19]. Our goal is not to use elimination to solve for the source location directly, but instead to gather information about the set of possible Doppler shifts and FDOA measurements.

7.2 Problem Formulation

The map F_3 was introduced in Chapter 2 for an emitter in $\mathbb{R}^3$. For simplicity, we now consider the map F_2 :

$$\begin{aligned} F_2: \quad \mathbb{R}^2 &\longrightarrow \mathbb{R}^2 \\ (x,y) &\longrightarrow (f_{1,2}, f_{1,3}). \end{aligned} \tag{7.1}$$

This takes the emitter location, (x, y), to a set of FDOA measurements in a system with three receivers. Recall that receiver locations, x_i, y_i, and velocities, u_i, v_i, are fixed parameters. The image of this map, denoted $Im(F_2)$, consists of all values $(f_{1,2}, f_{1,3})$ where there exists a corresponding $(x, y) \in \mathbb{R}^2$ that will be mapped to them. Thus, $Im(F_2)$ gives the set of all feasible FDOA measurements. We would like to find an algebraic expression for $Im(F_2)$, which would translate to a necessary condition that all sets of measurements $(f_{1,2}, f_{1,3})$ must satisfy. Unfortunately, for reasons that will be discussed in the next section this is not possible. Instead, since the FDOA values are equivalent to a difference of Doppler shifts, we

consider the Doppler shift map D_2 :

$$\begin{aligned} D_2: \quad \mathbb{R}^2 &\longrightarrow \mathbb{R}^3 \\ (x,y) &\longrightarrow (d_1,d_2,d_3), \end{aligned} \tag{7.2}$$

where d_1, d_2, and d_3 are given by

$$d_i = \frac{u_i(x-x_i)+v_i(y-y_i)}{\sqrt{(x-x_i)^2+(y-y_i)^2}}, \tag{7.3}$$

as introduced in Section 2.1.2. The maps D_2 and F_2 are closely related since $f_{1,2} = d_2 - d_1$ and $f_{1,3} = d_3 - d_1$. Thus, the image of F_2 is just a projection of the image of D_2:

$$(d_1,d_2,d_3) \xrightarrow{\begin{pmatrix} -1 & -1 \\ 1 & 0 \\ 0 & 1 \end{pmatrix}} (f_{12},f_{13}).$$

This means we are able to study the map D_2, then transfer the findings to the FDOA-based scenario. We can describe the image of D_2 algebraically and the set of all possible Doppler shifts (d_1, d_2, d_3) will form a surface in $\mathbb{R}^3$. We explore this further in the next section.

7.3 The Image of D_2

Let's step back and consider again the FDOA map (7.1). For the set of potential emitter locations to be zero-dimensional, the planar scenario requires three receivers and two independent FDOA measurements: $f_{1,2}$ and $f_{1,3}$ (see Table 3.1). The image of F_2 is two dimensional, since it is a mapping from $\mathbb{R}^2$ to $\mathbb{R}^2$ with no degeneracy. Since the dimension of the image of F_2 is equal to the dimension of its codomain, the image cannot be represented by a nonzero polynomial and thus is not an algebraic variety. This is because the dimension of an algebraic variety will always be strictly less than the dimension of the ambient space.

These dimensions are consistent with the TDOA case explored in [12] and explain why the set of feasible TDOA is not an algebraic set but instead a bounded region of $\mathbb{R}^2$.

This is the motivation for looking instead to D_2, the map of Doppler shifts. It essentially *lifts* a given set of FDOA measurements to a higher dimensional space. As stated above, the image of F_2 is a particular projection of the image of D_2. As an added benefit, the equations defining D_2 are algebraically simpler than the equations defining F_2. With a fixed set of parameters, we can map points forward with D_2 and F_2 to visualize their images. This is shown for three different sets of parameters in Figures 7.1, 7.2, and 7.3. Any point on the image is considered feasible, since there exists a corresponding real emitter position. Notice that the image of D_2 is a two-dimensional surface in the variables d_1, d_2 and d_3. We would like to find an algebraic expression to represent this surface of feasible measurements.

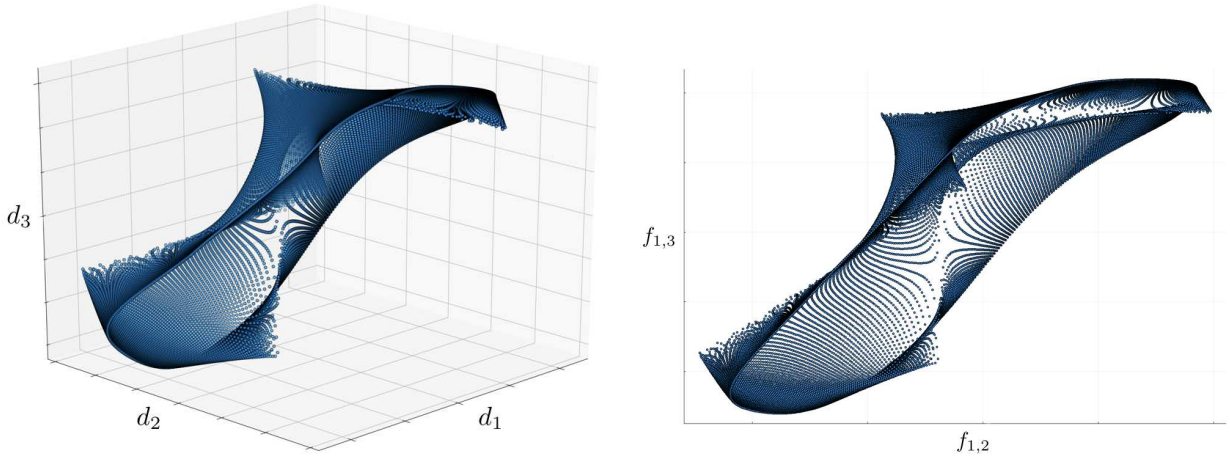

Figure 7.1: (Left) Points in the image of the map D_2 for fixed receiver position and velocities. (Right) Image of F_2 with the same parameters. Notice that the plot on the right is a projection of plot on the left since: $f_{1,2} = d_2 - d_1$ and $f_{1,3} = d_3 - d_1$.

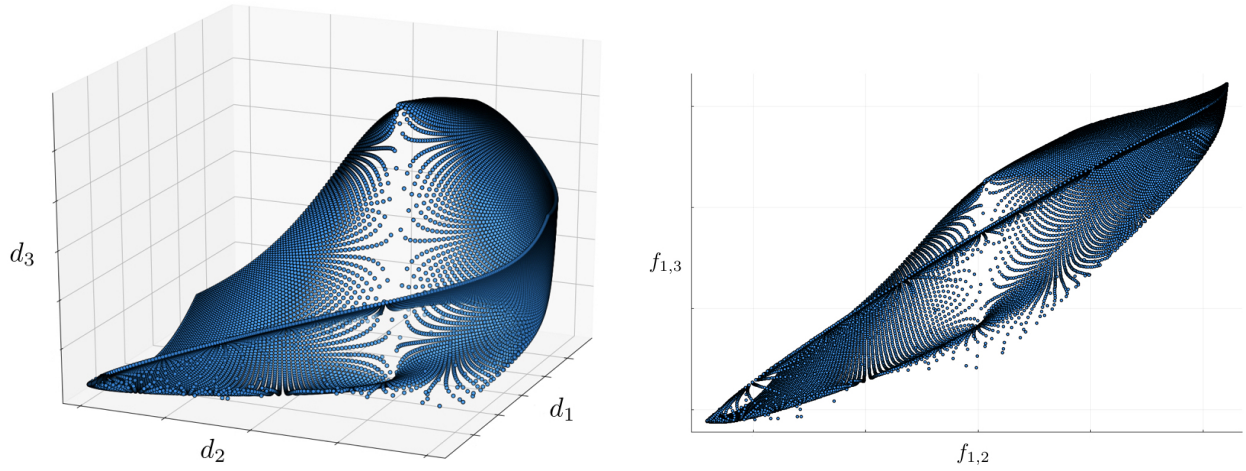

Figure 7.2: The content of this plot is the same as Figure 7.1 with different parameter values. Notice that the plot on the right is a projection of plot on the left since: $f_{1,2} = d_2 - d_1$ and $f_{1,3} = d_3 - d_1$.

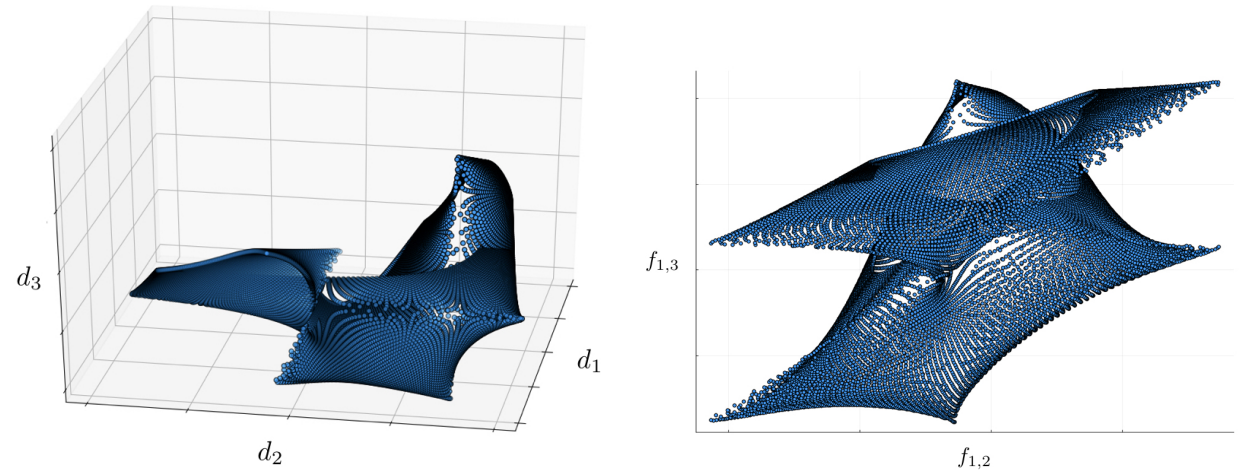

Figure 7.3: The content of this plot is the same as Figure 7.1 and Figure 7.2 with different parameter values. Notice that the plot on the right is a projection of plot on the left since: $f_{1,2} = d_2 - d_1$ and $f_{1,3} = d_3 - d_1$.

Converting D_2 to a set of polynomials allows the use of resultants and elimination theory. Squaring (7.3) and clearing the denominator, we get the Doppler shift polynomials:

$$p_1 = ((x - x_1)^2 + (y - y_1)^2)d_1^2 - (u_1(x - x_1) + v_1(y - y_1))^2$$
$$p_2 = ((x - x_2)^2 + (y - y_2)^2)d_2^2 - (u_2(x - x_2) + v_2(y - y_2))^2$$
$$p_3 = ((x - x_3)^2 + (y - y_3)^2)d_3^2 - (u_3(x - x_3) + v_3(y - y_3))^2.$$

There is one expression for each receiver (3 equations) with variables x, y, d_1, d_2, and d_3. We fix the parameters x_1, x_2, x_3, y_1, y_2, y_3, u_1, u_2, u_3, v_1, v_2, and v_3. We would like to find the surface defined by all possible (d_1, d_2, d_3). In other words, if $\mathcal{I} = \langle p_1, p_2, p_3 \rangle \subseteq \mathbb{Q}[x, y, d_1, d_2, d_3]$, what is $\mathcal{I} \cap \mathbb{Q}[d_1, d_2, d_3]$?

7.3.1 Elimination

Introduced in Section 4.2.3, resultants are useful for eliminating variables from one or more polynomial expressions. For a system of three polynomials, as above, one could repeatedly compute the Sylvester resultant for pairs of the equations, eliminating one variable at a time. However, there are other methods that are more computationally efficient for a system of this form. One of the fastest methods for computing resultants for variable elimination with multiple polynomials is the *Dixon resultant* [37], which falls into a class of methods known as multivariate resultants. We utilize one of several implementations, the DR package in Maple [30, 38].

Recall, the Sylvester resultant utilizes the fact that if two polynomials f and g have a common factor, there exist polynomials A and B such that:

$$Af + Bg = 0,$$

with a few additional conditions (Theorem 4 in Section 4.2.3). Now, the Dixon resultant takes advantage of a different condition that polynomials with a factor in common must satisfy. It is based on the fact that the polynomial

$$\delta(x,t) = \frac{1}{x-t}\det\begin{pmatrix} f(x) & g(x) \\ f(t) & g(t) \end{pmatrix} = \frac{f(x)g(t) - g(x)f(t)}{x-t}, \tag{7.4}$$

will be zero for any value x that is a common zero of f and g [37]. Here, t is an auxiliary variable and the polynomial $\delta(x,t)$ is referred to as the *Dixon polynomial*. This method generalizes to systems with multiple polynomials and variables with the addition of more auxiliary variables. From here, the Dixon resultant computation is carried out in a similar manner to that of the Sylvester resultant. A matrix of coefficients (*Dixon matrix*) is created whose determinant is zero when all polynomials have a common factor. Thus, the determinant of the Dixon matrix (*Dixon resultant*) gives an expression from which the desired variables have been eliminated. For a more complete discussion of these methods, see [30].

For the computation of $\mathcal{I} \cap \mathbb{Q}[d_1, d_2, d_3]$, we seek to use resultants to eliminate x and y from the ideal generated by p_1, p_2, and p_3. Computing the Dixon polynomial and corresponding Dixon matrix using the DR package in Maple is a relatively quick task and results in a 5×5 Dixon matrix. Because this matrix is small, we found that using the "Determinant" command with minor expansion in Maple to compute the determinant (the Dixon resultant) was faster than Dixon resultant extraction with the DR package. The resultant, after factoring out a single extraneous ellipsoid, was found to be a degree 20 polynomial in d_1, d_2, and d_3. The entire computation, including factoring, took well under a second.

The resulting degree 20 surface is shown in Figure 7.4. The numerical algebraic geometry software, Bertini [15], can be used to verify that this polynomial is indeed the resultant and contains no further extraneous factors. Bertini is able to find positive-dimensional components in a solution set, for instance curves or surfaces that satisfy a system of polynomials [28]. It provides information about the dimension and degree of each component, along with a set of points lying on the solution set. This set is referred to as a *witness set*. For the system above consisting of p_1, p_2, and p_3 with variables x, y, d_1, d_2, and d_3 and numerical parameter values, the solution set consists of a single algebraic surface (dimension

2) of degree 44. Bertini also has the capability to project away variables and return the dimension and degree of the corresponding projected algebraic variety.[8] This is analogous to performing variable elimination. When we project points in the solution set:

$$(x, y, d_1, d_2, d_3) \longrightarrow (d_1, d_2, d_3),$$

the result is a single degree 20 surface (now in the variables d_1, d_2, and d_3). This is consistent with the resultant.

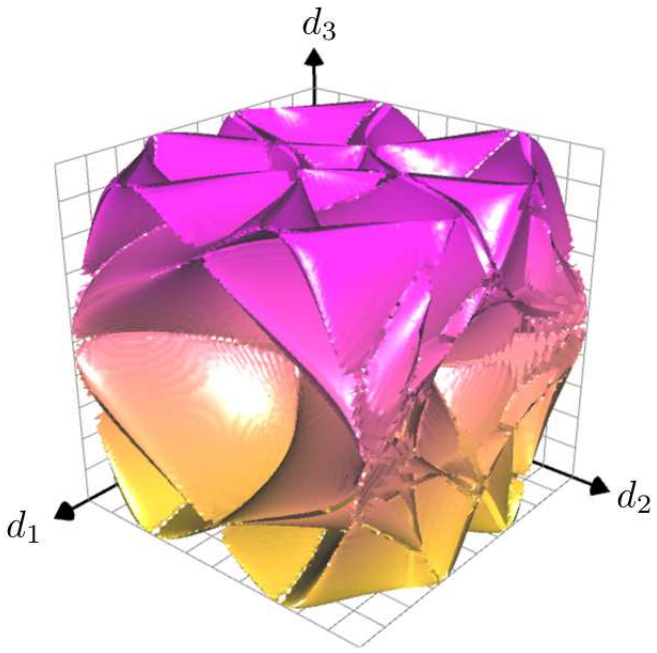

Figure 7.4: Surface for $\mathcal{I} \cap \mathbb{Q}[d_1, d_2, d_3]$ resulting from Dixon resultant computation. The parameters used to generate this surface are the same as those in Figure 7.1.

7.3.2 Discussion

Visually comparing Figure 7.4 and the left side of Figure 7.1, it is clear that the resultant is not equivalent to the image of D_2. While we can verify that every point in the image of D_2

[8] See Chapter 16 of [15] for more information.

satisfies the resultant, the converse is not true. The surface defined by the resultant includes many points that are not in the image of D_2 and thus do not define feasible Doppler shifts.

This discrepancy is primarily caused by the squaring of each equation to create the polynomial system defined by p_1, p_2, and p_3. Indeed, the resultant does not include only points from $Im(D_2)$:

$$(x, y) \longrightarrow (\ d_1,\ d_2,\ d_3)$$

but also points defined by seven other maps:

$$\begin{aligned}
(x, y) &\longrightarrow (-d_1,\ \ d_2,\ \ d_3) \\
(x, y) &\longrightarrow (\ \ d_1, -d_2,\ \ d_3) \\
&\vdots \\
(x, y) &\longrightarrow (-d_1, -d_2, -d_3).
\end{aligned}$$

This means that the resultant consists of 2^3 copies of the surface in Figure 7.1.

This does not change the fact that the variety corresponding to the resultant is the smallest algebraic variety containing $Im(D_2)$, referred to as the *Zariski closure* of $Im(D_2)$. If we want to use the surface, for instance for de-noising purposes, it is necessary to find a way to distinguish between sections of the resultant. We would like to identify whether a point on the surface corresponds to a truly feasible Doppler shift.

We are interested in how the FDOA case compares to a similar analysis of the TDOA-based scenario. The surface of feasible Doppler shifts, given by a degree 20 polynomial, is more complicated than the range map surface found in [13], defined by a polynomial of degree 4. Additionally, the range map surface has a section in each octant, only one of which is relevant to the TDOA problem. Thus, the surface can be reduced to just the section lying in the first octant. Projecting this section of the range map surface to the TDOA space is a 1-to-1 map, with some 1-to-2 regions, and fills a convex region of $\mathbb{R}^2$ [13]. Comparatively, the

projection of $Im(D_2)$ or the Doppler shift surface (Figure 7.4) to obtain bounds for FDOA measurements is not a 1-to-1 map and the resulting region is not convex. In fact, a set of FDOA measurements has been found to have as many as six corresponding feasible emitter locations. This complexity can be seen in the right side of Figures 7.1, 7.2, and 7.3.

7.4 Conclusion

Using tools from elimination theory, we are able to identify the surface of feasible Doppler shifts as being defined by a degree 20 polynomial equation. While this does give a necessary condition that Doppler shifts must satisfy, we often do not have access to the observed Doppler shifts, only their differences (FDOA). Additionally, the surface defined by the polynomial contains sections that are not in the image of the Doppler shift map. These extraneous sections arise from the squaring of (7.3) to remove square roots. Unfortunately, this means that projecting the Doppler shift surface to the FDOA space will indicate a larger region of feasible FDOA than is actually the case. Additionally, there is no apparent way of separating out the 'correct' region from the rest of the Doppler shift surface. This indicates that obtaining and utilizing the region of feasible FDOA is much less straightforward than the comparable TDOA case.

Chapter 8

Conclusion and Future Work

8.1 Conclusion

The broad goal of this thesis was to demonstrate how techniques from mathematics, particularly algebraic geometry, can be useful for tackling the interesting geometry of FDOA-based source localization. This culminated in three separate projects, each of which approached the source localization problem from a slightly different angle.

Formulating the problem as a polynomial system (Chapter 3) allowed for the utilization of polynomial solvers from numerical algebraic geometry. With these tools we are able to find all zero-dimensional solutions to the FDOA (or TDOA) polynomial system up to a designated numerical accuracy. Combining this capability with the iterative process, RANSAC, provided methods for handling noise and measurement error. These concepts build the framework for the FDOA-RANSAC algorithm developed in Chapter 5.

In addition to TDOA and FDOA measurements, the direction of arrival (DOA) is a helpful quantity for locating a source. When a source is in the far-field, the resulting FDOA measurements lie on an ellipse determined by the receiver velocities (Chapter 6). This is an interesting relationship that allows for the estimation of the direction of arrival from a set of FDOA or TDOA measurements.

Formulating the FDOA-based source localization problem as a polynomial system also allows for the use of methods from elimination theory. With the elimination of variables, we find that all Doppler shifts corresponding to a given receiver configuration lie on an algebraic surface defined by a degree 20 polynomial equation (Chapter 7). This provides a necessary condition that all Doppler shifts must satisfy and provides a basis for understanding the closely-related set of feasible FDOA measurements.

These projects provide insight into three separate aspects of FDOA-base source localization. While the first two projects lead to direct methods for finding the location of a source, the last project approaches the problem from a more theoretical perspective and seeks to better understand the complex role that the Doppler shift plays in source localization.

8.2 Future Work

Passive source localization is a mathematically rich and practically valuable area. Thus, there are several directions in which this research could be extended in the future. Two potential projects relating to this dissertation are summarized below.

8.2.1 De-noising with the Set of Feasible FDOA

The exploration of the Doppler shift surface in Chapter 7 is the first step toward developing an algorithm for the de-noising of FDOA measurements. There are a few different potential approaches to this project. In the TDOA de-noising algorithm developed in [14], the authors identify the set of feasible TDOA as a convex bounded region of $\mathbb{R}^2$. This is the projection of the range map surface onto the TDOA space. Thus, de-noising of TDOA measurements is performed by minimizing the distance between noisy measurements and this feasible set. Unfortunately, in the FDOA case, the projection of the Doppler shift surface to the FDOA space contains additional regions that do not correspond to feasible FDOA measurements. Thus, minimizing the distance between this set and noisy measurements will not be an effective method for de-noising.

Another approach to de-noising is to first lift a noisy measurement to a line of Doppler shifts. Then this line can be projected to the algebraic surface of feasible Doppler shifts. Methods for the projection to algebraic sets have been established, although in a different context [39, 40]. Thus, this is a promising alternative to the method above, although there is still an issue with the Doppler shift surface containing sections that do not actually correspond to feasible Doppler shifts.

8.2.2 Emitter in Motion

One assumption of the model we have used thus far is that the signal's source is stationary. However, in practical application this is often not the case. Consider for example the problem of locating a ship in distress in the ocean. The ship is very likely to be moving; whether bobbing up and down or drifting with currents. Emitter motion affects the Doppler shift formula by adding an additional vector-valued variable, $\mathbf{v}_0$, velocity of the emitter. Thus the Doppler shift becomes:

$$d_i = \frac{f_0}{c}\left((\mathbf{v}_i - \mathbf{v}_0) \cdot \frac{\mathbf{x} - \mathbf{x}_i}{\|\mathbf{x} - \mathbf{x}_i\|}\right).$$

When the emitter was assumed to be stationary, the relative velocity between receiver and emitter was equivalent to $\mathbf{v}_i$. Now, adding the possibility for emitter motion, the relative velocity is equivalent to the difference $\mathbf{v}_i - \mathbf{v}_0$. The addition of this extra set of variables means that more observations are needed to obtain a zero-dimensional solution set.

Bibliography

[1] NOAA Search and rescue satellite aided tracking (SARSAT). `http://www.sarsat.noaa.gov/`, 2018.

[2] X. Alameda-Pineda and R. Horaud. A geometric approach to sound source localization from time-delay estimates. *IEEE/ACM Transactions on Audio, Speech, and Language Processing*, 22(6):1082–1095, June 2014.

[3] H. D. Griffiths and C. J. Baker. *An Introduction to Passive Radar (Artech House Radar)*. Artech House, 2017.

[4] M. Cheney and B. Borden. *Fundamentals of Radar Imaging*. Society for Industrial and Applied Mathematics, 2009.

[5] H. Schau and A. Robinson. Passive source localization employing intersecting spherical surfaces from time-of-arrival differences. *IEEE Transactions on Acoustics, Speech, and Signal Processing*, 35(8):1223–1225, Aug 1987.

[6] Y. T. Chan and K. C. Ho. An efficient closed-form localization solution from time difference of arrival measurements. In *Acoustics, Speech, and Signal Processing, 1994. ICASSP-94., 1994 IEEE International Conference on*, volume ii, pages II/393–II/396 vol.2, Apr 1994.

[7] R. Schmidt. Least squares range difference location. *IEEE Transactions on Aerospace and Electronic Systems*, 32(1):234–242, Jan 1996.

[8] K. C. Ho and Y. T. Chan. Geolocation of a known altitude object from TDOA and FDOA measurements. *IEEE Transactions on Aerospace and Electronic Systems*, 33(3):770–783, July 1997.

[9] S. R. Drake and K. Dogancay. Geolocation by time difference of arrival using hyperbolic asymptotes. In *2004 IEEE International Conference on Acoustics, Speech, and Signal Processing*, volume 2, pages ii–361–4 vol.2, May 2004.

[10] S. J. Spencer. Closed-form analytical solutions of the time difference of arrival source location problem for minimal element monitoring arrays. *The Journal of the Acoustical Society of America*, 127(5):2943–2954, 2010.

[11] L. A. Romero and J. Mason. Evaluation of direct and iterative methods for overdetermined systems of TOA geolocation equations. *IEEE Transactions on Aerospace and Electronic Systems*, 47(2):1213–1229, April 2011.

[12] M. Compagnoni, R. Notari, F. Antonacci, and A. Sarti. A comprehensive analysis of the geometry of TDOA maps in localization problems. *Inverse Problems*, 30(3), 2014.

[13] M. Compagnoni, R. Notari, A. A. Ruggiu, F. Antonacci, and A. Sarti. The algebro-geometric study of range maps. *arXiv:1604.08076*, 2016.

[14] M. Compagnoni, A. Canclini, P. Bestagini, F. Antonacci, A. Sarti, and S. Tubaro. Source localization and denoising: a perspective from the TDOA space. *Multidimensional Systems and Signal Processing*, 28(4):1283–1308, Oct 2017.

[15] D. Bates, J. Hauenstein, A. Sommese, and C. Wampler. *Numerically solving polynomial systems with Bertini*. Society for Industrial and Applied Mathematics, 2013.

[16] J. S. Abel. A divide and conquer approach to least-squares estimation. *IEEE Transactions on Aerospace and Electronic Systems*, 26(2):423–427, Mar 1990.

[17] P. Li and X. Ma. *Robust Acoustic Source Localization with TDOA Based RANSAC Algorithm*, pages 222–227. Springer Berlin Heidelberg, Berlin, Heidelberg, 2009.

[18] D. J. Torrieri. Statistical theory of passive location systems. *IEEE Transactions on Aerospace and Electronic Systems*, AES-20(2):183–198, March 1984.

[19] J. Mason and L. Romero. TOA/FOA geolocation solutions using multivariate resultants. *Navigation*, 52(3):163–177, 2005.

[20] J. L. Awange and E. W. Grafarend. Algebraic solution of GPS pseudo-ranging equations. *GPS Solutions*, 5(4):20–32, Apr 2002.

[21] J. Smith and J. Abel. Closed-form least-squares source location estimation from range-difference measurements. *IEEE Transactions on Acoustics, Speech, and Signal Processing*, 35(12):1661–1669, Dec 1987.

[22] M. S. Brandstein, J. E. Adcock, and H. F. Silverman. A closed-form method for finding source locations from microphone-array time-delay estimates. In *1995 International Conference on Acoustics, Speech, and Signal Processing*, volume 5, pages 3019–3022 vol.5, May 1995.

[23] S. Shuster, A. J. Sinclair, and T. A. Lovell. Initial relative-orbit determination using heterogeneous TDOA. In *2017 IEEE Aerospace Conference*, pages 1–7, March 2017.

[24] J. Li, F. Guo, and W. Jiang. A linear-correction least-squares approach for geolocation using fdoa measurements only. *Chinese Journal of Aeronautics*, 25(5):709 – 714, 2012.

[25] E. L. Allgower and K. Georg. *Introduction to Numerical Continuation Methods*. SIAM, Philadelphia, 2003.

[26] T. R. Chen, T. Y. Li, and T. L. Lee. *Hom4PS-3 is a parallel software package specialized for solving system of polynomial equations using efficient and reliable numerical methods.* 2015.

[27] J. Verschelde. *PHCpack: a general-purpose solver for polynomial systems by homotopy continuation.* ACM Trans Math Software 25:251276., 2015.

[28] A.J. Sommese and C.W. Wampler. *Numerical solution of polynomial systems arising in engineering and science*. World Scientific, Singapore, 2005.

[29] D. A. Cox, J. Little, and D. O'Shea. *Ideals, Varieties, and Algorithms: An Introduction to Computational Algebraic Geometry and Commutative Algebra, 3/e (Undergraduate Texts in Mathematics)*. Springer-Verlag, Berlin, Heidelberg, 2007.

[30] M. Minimair. Computing the dixon resultant with the Maple package DR. In Ilias S. Kotsireas and Edgar Martínez-Moro, editors, *Applications of Computer Algebra*, pages 273–287, Cham, 2017. Springer International Publishing.

[31] K. J. Cameron and D. J. Bates. Geolocation with FDOA measurements via polynomial systems and RANSAC. In *2018 IEEE Radar Conference (RadarConf18)*, pages 0676–0681, April 2018.

[32] M. A. Fischler and R. C. Bolles. Random sample consensus: A paradigm for model fitting with applications to image analysis and automated cartography. *Commun. ACM*, 24(6):381–395, June 1981.

[33] T. Urbančič, M. Fras, B. Stopar, and K. Božo. *The Influence of the Input Parameters Selection on the RANSAC Results*, volume 13, pages 159–170. 06 2014.

[34] K. J. Cameron and S. J. Pine. A novel method for determining DOA from far-field TDOA or FDOA. arXiv:1808.04741, 2018.

[35] J. Benesty. *Direction-of-Arrival and Time-Difference-of-Arrival Estimation*, pages 181–215. Springer Berlin Heidelberg, Berlin, Heidelberg, 2008.

[36] Introduction into the theory of direction finding. In *Radiomonitoring & Radiolocation Catalog*, pages 61–112. Rohde and Schwarz, 2016.

[37] A. L. Dixon. The eliminant of three quantics in two independent variables. *Proceedings of the London Mathematical Society*, s2-7(1):49–69, 1908.

[38] Maple 2017. Maplesoft, a division of Waterloo Maple Inc. Waterloo, Ontario.

[39] J. D. Hauenstein. Numerically computing real points on algebraic sets. *Acta Applicandae Mathematicae*, 125(1):105–119, Jun 2013.

[40] E. Gross, B. Davis, K. L. Ho, D. J. Bates, and H. A. Harrington. Numerical algebraic geometry for model selection and its application to the life sciences. *Journal of The Royal Society Interface*, 13(123), 2016.

[41] M. Pourhomayoun and M. L. Fowler. Exploiting cross ambiguity function properties for data compression in emitter location systems. In *2011 45th Annual Conference on Information Sciences and Systems*, pages 1–5, March 2011.

[42] D. Nelson. Locating emitters using a cross-spectral cross-ambiguity function (CSCAF). 8391:7–18, 05 2012.

Appendix A

Calculating TDOA and FDOA

The majority of this paper develops methods for using TDOA and FDOA measurements to locate an emitter. Or, it seeks to answer the question: given a set of measurements, where did the signal originate? However, for context, some notes should also be made about the signal processing techniques used to obtain the measurements $\tau_{i,j}$ and $f_{i,j}$.

Consider the calculation of TDOA and FDOA between receivers 1 and 2. Receiver 1 collects an incoming signal $s_1(t)$ and receiver 2 collects an incoming signal $s_2(t)$. Each of these signals is equivalent to the sent signal, $s(t)$, up to a time delay and a frequency shift. Mathematically,

$$s_1(t) = s(t - \tau_1)e^{-id_1(t-\tau_1)}$$
$$s_2(t) = s(t - \tau_2)e^{-id_2(t-\tau_2)},$$

with time delay τ_i and frequency shifts f_i.

The time delay and frequency shift between the two received signals can be calculated by performing a correlation of $s_1(t)$ with a time and frequency shifted version of $s_2(t)$. This is done using the cross ambiguity function (CAF). The function is defined mathematically [41] as

$$CAF(\tau, f) = \int_0^T s_1^*(t)\ s_2(t + \tau)\ e^{ift}\ dt,$$

where $*$ denotes the complex conjugate and τ and f represent the imposed time and frequency shift, respectively. For the two signals above,

$$CAF(\tau, f) = \int_0^T s^*(t-\tau_1)\; s(t+\tau-\tau_2)\; e^{id_1(t-\tau_1)}\; e^{-id_2(t-\tau_2)}\; e^{ift}\; dt$$
$$= \int_0^T s^*(t-\tau_1)\; s(t-\tau_2+\tau)\; e^{-i(d_2-d_1-f)t}\; dt \;\cdot\; e^{i(d_2\tau_2-d_1\tau_1)}. \qquad \text{(A.1)}$$

This is simply an inner product between $s_1(t)$ and the modified $s_2(t)$. One key property that follows is that the magnitude,

$$|CAF(\tau, f)| = |\left\langle s^*(t-\tau_1), s(t-\tau_2+\tau)\; e^{-i(d_2-d_1-f)t} \right\rangle|,$$

will be largest at the (τ, f) values corresponding to the time delay and frequency shift between the two signals [42]. This can be proven with the Cauchy-Schwarz inequality. The magnitude of the inner product is largest when both sides (waveforms in this case) are equivalent. This is achieved when $\tau = \tau_2 - \tau_1 = \tau_{1,2}$. Additionally, $e^{-i(d_2-d_1-f)t} = 1$ when $f = d_2 - d_1 = f_{1,2}$.

Thus, evaluating (A.1) for various values of τ and f and taking the magnitude forms a surface whose peak corresponds to the TDOA and FDOA. An example of this surface is shown in Figure A.1. Based on the type of signal received, the cross ambiguity surface may be broad in the range or frequency directions, making it difficult to accurately find the maximum. In fact, the radar uncertainty principle states that range resolution and Doppler resolution are inversely related: an increase in one will lead to a decrease in the other [4]. The cross ambiguity function shown in Figure A.2 demonstrates a case with high FDOA accuracy and low TDOA accuracy. This is a motivation for developing better methods for geolocation using TDOA *or* FDOA; different signals will be more accurate in one type of measurement or the other.

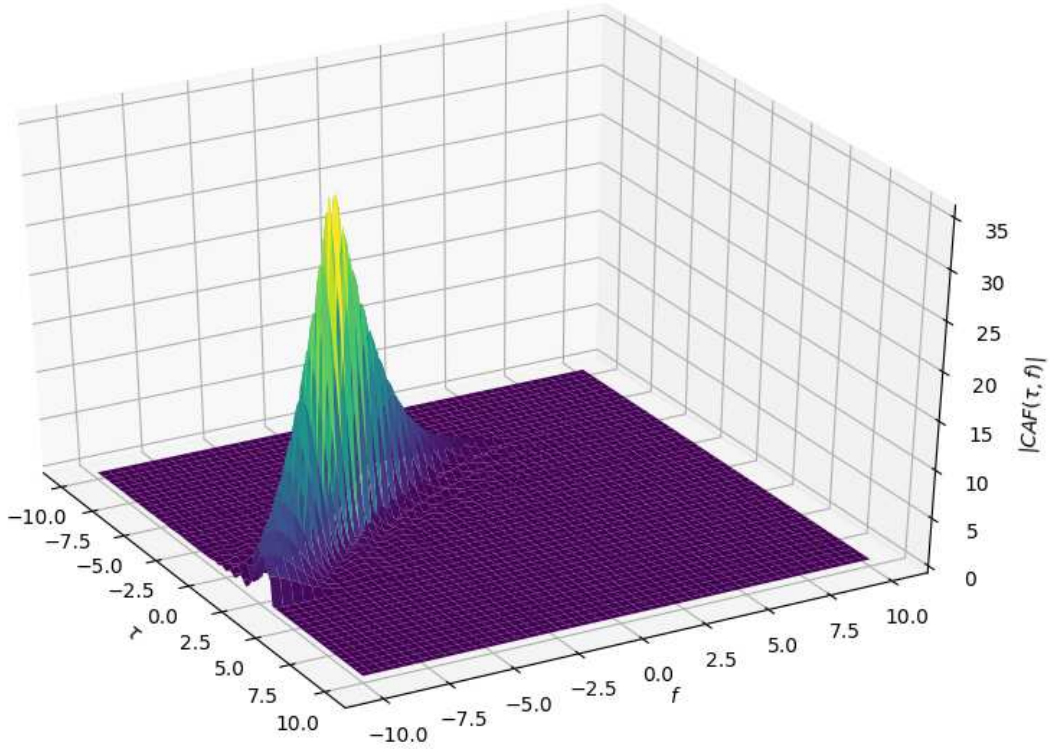

Figure A.1: Cross ambiguity function for a linear chirp. The correct TDOA is $\tau = -1$ and the FDOA is $f = -5$.

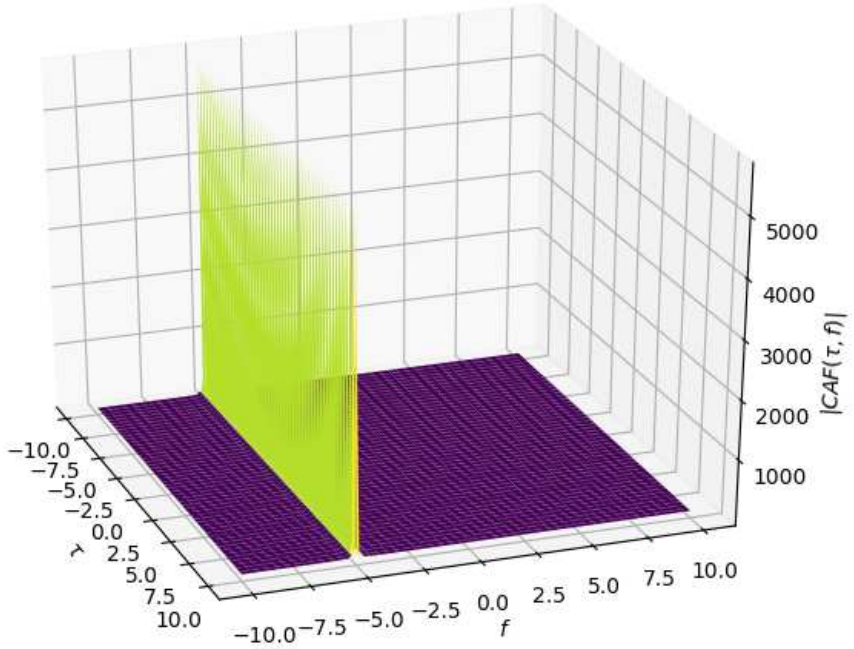

Figure A.2: Cross ambiguity function for a continuous wave signal. As above, the correct TDOA is $\tau = -1$ and the FDOA is $f = -5$. Note that this signal results in coarse TDOA resolution and fine FDOA resolution. Thus, the FDOA estimate has a higher level of accuracy than the TDOA estimate.

Appendix B

FDOA System: Measurements Taken over Multiple Time Steps

If receivers are allowed to take measurements over multiple time steps, the polynomial systems given in Chapter 3 can be altered slightly to involve measurements from a *single pair* of receivers at n time steps. This leads to a variation of Table 3.1, now with bounds on the number of measurements needed for the solution set to be finite. This is the content of Table B.1. It is easy to see how these numbers are obtained since a system with 4 receivers results in 3 linearly independent measurements, 3 receivers result in 2 measurements, etc. Thus, considering the FDOA system in 3D with a single receiver, we specifically consider the case with $n = 3$ measurements, since this will result in a finite solution set with probability one. This system is:

$$
\begin{aligned}
r_{a,1}r_{b,1}f_1 \;-\; & r_{a,1}\left[u_{b,1}(x_{b,1}-x)+v_{b,1}(y_{b,1}-y)+w_{b,1}(z_{b,1}-z)\right] \\
& +\; r_{b,1}\left[u_{a,1}(x_{a,1}-x)+v_{a,1}(y_{a,1}-y)+w_{a,1}(z_{a,1}-z)\right]=0 \\
r_{a,2}r_{b,2}f_2 \;-\; & r_{a,2}\left[u_{b,2}(x_{b,2}-x)+v_{b,2}(y_{b,2}-y)+w_{b,2}(z_{b,2}-z)\right] \\
& +\; r_{b,2}\left[u_{a,2}(x_{a,2}-x)+v_{a,2}(y_{a,2}-y)+w_{a,2}(z_{a,2}-z)\right]=0 \\
r_{a,3}r_{b,3}f_3 \;-\; & r_{a,3}\left[u_{b,3}(x_{b,3}-x)+v_{b,3}(y_{b,3}-y)+w_{b,3}(z_{b,3}-z)\right] \\
& +\; r_{b,3}\left[u_{a,3}(x_{a,3}-x)+v_{a,3}(y_{a,3}-y)+w_{a,3}(z_{a,3}-z)\right]=0
\end{aligned}
$$

$$
\begin{aligned}
& r_{a,1}^2-(x^2+y^2+z^2)-(x_{a,1}^2+y_{a,1}^2+z_{a,1}^2)+2(x_{a,1}x+y_{a,1}y+z_{a,1}z)=0 \\
& r_{b,1}^2-(x^2+y^2+z^2)-(x_{b,1}^2+y_{b,1}^2+z_{b,1}^2)+2(x_{b,1}x+y_{b,1}y+z_{b,1}z)=0 \\
& r_{a,2}^2-(x^2+y^2+z^2)-(x_{a,2}^2+y_{a,2}^2+z_{a,2}^2)+2(x_{a,2}x+y_{a,2}y+z_{a,2}z)=0 \\
& r_{b,2}^2-(x^2+y^2+z^2)-(x_{b,2}^2+y_{b,2}^2+z_{b,2}^2)+2(x_{b,2}x+y_{b,2}y+z_{b,2}z)=0 \\
& r_{a,3}^2-(x^2+y^2+z^2)-(x_{a,3}^2+y_{a,3}^2+z_{a,3}^2)+2(x_{a,3}x+y_{a,3}y+z_{a,3}z)=0 \\
& r_{b,3}^2-(x^2+y^2+z^2)-(x_{b,3}^2+y_{b,3}^2+z_{b,3}^2)+2(x_{b,3}x+y_{b,3}y+z_{b,3}z)=0.
\end{aligned}
$$

The receivers are now given letters a and b, and time steps are numbered 1-3.

Table B.1: Minimum number of TDOA and FDOA measurements necessary to reduce set of potential transmitter locations to a finite number, for varying dimensions (2 or 3) and types of measurements being used.

	# measurements (2D)	# measurements (3D)
TDOA only	2	3
TDOA + ALT	-	2
FDOA only	2	3
FDOA + ALT	-	2
TDOA + FDOA	1	2
TDOA + FDOA + ALT	-	1